

TABLE 1. Correlation function parameters, semi-volume limited samples.

Sample	s_0 (h^{-1} Mpc)	γ_s	σ_8	r_0 (h^{-1} Mpc)	γ_r	σ_8
(1)	(2)	(3)	(4)	(5)	(6)	(7)
South	5.80 ± 0.19	1.65 ± 0.11	0.99 ± 0.03	5.12 ± 0.37	1.99 ± 0.22	0.96 ± 0.07
North	5.62 ± 0.22	1.66 ± 0.15	0.97 ± 0.04	6.01 ± 0.44	1.82 ± 0.19	1.06 ± 0.08
Combined	5.85 ± 0.13	1.60 ± 0.08	0.99 ± 0.02	5.36 ± 0.33	1.86 ± 0.16	0.96 ± 0.06

Southern Sky Redshift Survey: Clustering of Local Galaxies ¹

C. N. A. Willmer

Observatório Nacional, Rua General José Cristino 77, Rio de Janeiro, RJ 20921-030, Brazil
 electronic mail: cnaw@on.br

L. Nicolaci da Costa ²

European Southern Observatory, Karl-Schwarzschild Str. 2, Garching-bei-München, Germany
 electronic mail: ldacosta@eso.org

and

P. S. Pellegrini

Observatório Nacional, Rua General José Cristino 77, Rio de Janeiro, RJ 20921-030, Brazil
 electronic mail: pssp@on.br

ABSTRACT

We use the two-point correlation function to calculate the clustering properties of the recently completed SSRS2 survey, which probes two well separated regions of the sky, allowing one to evaluate the sensitivity of sample-to-sample variations. Taking advantage of the large number of galaxies in the combined sample, we also investigate the dependence of clustering on the internal properties of galaxies.

The redshift space correlation function for the combined magnitude-limited sample of the SSRS2 is given by $\xi(s) = (s/5.85 h^{-1} \text{ Mpc})^{-1.60}$ for separations between $2 \leq s \leq 11 h^{-1} \text{ Mpc}$, while our best estimate for the real space correlation function is $\xi(r) = (r/5.36 h^{-1} \text{ Mpc})^{-1.86}$. Both are comparable to previous measurements using surveys of optical galaxies over much larger and independent volumes. By comparing the correlation function calculated in redshift and real space we find that the redshift distortion on intermediate scales is small. This result implies that the observed redshift-space distribution of galaxies is close to that in real space, and that $\beta = \Omega^{0.6}/b < 1$, where Ω is the cosmological density parameter and b is the linear biasing factor for optical galaxies.

¹Based on observations at Cerro Tololo Interamerican Observatory (CTIO), National Optical Astronomy Observatories (NOAO) which is operated by the Association of Universities for Research in Astronomy, Inc. under contract to the National Science Foundation; Complejo Astronomico El Leoncito (CASLEO), operated under agreement between the Consejo Nacional de Investigaciones Científicas de la República Argentina and the National Universities of La Plata, Córdoba and San Juan; European Southern Observatory (ESO), partially under the ESO-ON agreement; Laboratório Nacional de Astrofísica; and the South African Astronomical Observatory

²Observatório Nacional, Rua General José Cristino 77, Rio de Janeiro, RJ 20921-030, Brazil.

We have used the SSRS2 sample to study the dependence of ξ on the internal properties of galaxies such as luminosity, morphology and color. We confirm earlier results that luminous galaxies ($L > L^*$) are more clustered than sub- L^* galaxies and that the luminosity segregation is scale-independent. We also find that early types are more clustered than late types. However, in the absence of rich clusters, the relative bias between early and late types in real space, $b_{E+S0}/b_S \sim 1.2$, is not as strong as previously estimated. Furthermore, both morphologies present a luminosity-dependent bias, with the early types showing a slightly stronger dependence on the luminosity. We also find that red galaxies are significantly more clustered than blue ones, with a mean relative bias of $b_R/b_B \sim 1.4$, stronger than that seen for morphology. Finally, by comparing our results with the measurements obtained from the infrared-selected galaxies we determine that the relative bias between optical and *IRAS* galaxies in real space is $b_o/b_I \sim 1.4$.

Subject headings: cosmology: observations – galaxies: large-scale structure – galaxies: clustering

1. Introduction

Optical surveys using full sampling (CfA2, Geller & Huchra, 1989; SSRS2, da Costa et al. 1994, 1997) now probe over 30% of the sky down to a magnitude limit of $m_B = 15.5$. These surveys allow delineating various large-scale structures in the different volumes, thanks to their wide angular coverage. The combination of the large number of galaxies, complete sampling and sky coverage makes these surveys extremely useful to study some of the statistical properties of galaxy clustering. Thus, it becomes possible to divide the sample in bins of luminosities, morphologies and colors and study the dependence of clustering on these parameters.

The simplest characterization of the galaxy clustering can be expressed in terms of the two-point correlation function ξ . This statistic has been widely applied to a variety of samples which include surveys of optical (e.g., Davis & Peebles 1983; Davis et al. 1988; de Lapparent et al. 1988; Pellegrini et al. 1990*b*; Santiago & da Costa 1990; Loveday et al. 1995; Marzke et al. 1995; Hermit et al. 1996; Tucker et al. 1997; Guzzo et al. 1997) and *IRAS* galaxies (e.g., Davis et al. 1988; Saunders et al. 1992; Strauss et al. 1992; Fisher et al. 1994). The two-point correlation function has also been used to characterize the dependence of the galaxy clustering on the internal properties of galaxies such as morphology (e.g., Davis & Geller 1976; Giovanelli, Haynes & Chincarini 1986; Iovino et al. 1993; Loveday et al. 1995; Hermit et al. 1996; Guzzo et al. 1997), color (Tucker et al. 1996), surface brightness (Santiago & da Costa 1990), luminosity (e.g., Benoist et al. 1996 and references therein; Valotto & Lambas 1997; Guzzo et al. 1997) and internal dynamics (White, Tully & Davis 1988). However, since most samples analyzed so far have been relatively small, the quantitative results are by and large tentative.

In this paper we use the SSRS2 to investigate the correlation properties of galaxies in the nearby Universe, comparing our results with those obtained in other LCRS surveys such as the Stromlo-APM (Loveday et al. 1995), Las Campanas Redshift Survey (LCRS, Tucker et al. 1997) and *IRAS* (Fisher et al. 1994). We also measure how sensitive our results are to sample-to-sample variations. With our enlarged sample, we re-examine the luminosity dependence of ξ , previously studied by Benoist et al. (1996) who only used the southern galactic cap portion of the SSRS2. Finally, we investigate the dependence of the correlation properties on morphologies and colors. This information is a key ingredient for studies of galaxy biasing.

In Section 2 we describe the different catalogs we analyzed, while in Section 3 we describe the method used to compute the two-point correlation function in redshift and real space. In Section 4 we present the results we obtain for magnitude-limited samples. In Section 5 we examine the dependence of clustering on internal properties of galaxies, while in Section 6 we compare the correlation properties of our optical sample with the infrared-selected *IRAS* 1.2 Jy survey (Fisher et al. 1994). A summary is presented in Section 7.

2. Data

In this work we use data obtained for the SSRS2, which contains 5512 galaxies in both galactic hemispheres. The data are discussed in greater detail by da Costa et al. (1994; 1997) so only a brief description will be made here. The SSRS2 is extracted from the list of non-stellar objects in the Hubble Space Telescope Guide Star Catalog (Lasker et al. 1990, hereafter GSC). The SSRS2 is a complete catalog which is magnitude-limited at $m_B = 15.5$. Alonso et al. (1994) have shown that the galaxy magnitudes derived from the GSC are on a uniform isophotal magnitude system ($\sim 26 \text{ mag arc sec}^{-2}$) with estimated magnitude errors $\sim 0.3 \text{ mag}$. The SSRS2 south contains 3573 galaxies distributed over 1.13 steradians of the southern galactic cap ($b \leq -40^\circ$), within the declination range $-40^\circ \leq \delta \leq -2.5^\circ$. The SSRS2 north contains 1939 galaxies distributed over a solid angle of 0.57 steradians with $\delta \leq 0^\circ$ with $b \geq +35^\circ$. As described by da Costa et al. (1997) the galaxy morphologies in this sample used classifications based on other works (e.g., Lauberts & Valentijn 1989) as well as those made by the authors.

In this work we also considered a sub-sample of SSRS2 galaxies which have measured colors. For this we used the Lauberts & Valentijn (1989) catalog, so that the subcatalog of galaxies with colors only contains objects south of $\delta \approx -17.5^\circ$, in both galactic hemispheres. We also imposed a cut at $m_B = 14.5$ because beyond this magnitude the Lauberts & Valentijn (1989) catalog becomes incomplete, in particular for early type galaxies (Pellegrini et al. 1990a). This selection effect is caused by the fact that the Lauberts & Valentijn (1989) catalog is derived from the diameter-limited Lauberts (1982) catalog. The sample limited at $m_B=14.5$ contains 780 galaxies in both galactic hemispheres, of which 694 (89%) have colors. As pointed out by Marzke & da Costa (1997), this sample presents no systematic dependence of the color completeness with magnitude down to the 14.5 limit of this sub-sample.

All galaxy heliocentric velocities, v_\odot , have been corrected for the Solar motion with respect to the centroid of the Local Group using $v = v_\odot + 300 \sin(l) \cos(b) \text{ kms}^{-1}$, where (l, b) are the galactic coordinates of the galaxy. We also remove from the analyses all galaxies with radial velocities less than 500 kms^{-1} , as the redshifts for these objects are likely to be dominated by their peculiar velocities. We use throughout $H_o = 100 h \text{ kms}^{-1} \text{ Mpc}^{-1}$.

3. The Two-Point Correlation Function

3.1. Method

The two-point correlation function $\xi(r)$ can be computed from the data using the estimator suggested by Hamilton (1993):

$$\xi(r) = \frac{DD(r)RR(r)}{[DR(r)]^2} - 1, \quad (1)$$

where $DD(r)$, $RR(r)$ and $DR(r)$ are the number of data–data, random–random and data–random pairs, with separations in the interval between r and $r + dr$. The random catalog is generated using the same selection criteria as the galaxy sample. This estimator has the advantage that it is not too sensitive to uncertainties in the mean density, which is only a second order effect. The counts $DD(r)$, $DR(r)$ and $RR(r)$ can be generalized to include a weight w which is particularly important to correct for selection effects at large distances in magnitude-limited samples:

$$DD(r) = \sum_{i} \sum_{j}^{N_{gal} N_{gal}} w(s_j, r) w(s_i, r), \quad (2)$$

$$r - \Delta r \leq |s_i - s_j| \leq r + \Delta r$$

where i sums over all objects in the sample and the sum over j includes all particles at a distance s from the origin, which in this work is taken as the centroid of the Local Group, and $r = |\mathbf{s}_i - \mathbf{s}_j|$ is the separation of the pair (i, j) . The galaxy-random pairs $DR(r)$ and random-random pairs $RR(r)$ are similarly weighted. The most common weighting schemes are: equally weighted pairs $w(s_i, r) = 1$; equally-weighted volumes where $w(s_i, r) = 1/\phi(s_i)$ and the minimum variance weighting given by

$$w(s_i, r) = \frac{1}{1 + 4\pi\bar{n}J_3(r)\phi(s_i)}, \quad J_3(r) = \int_0^r dr' r'^2 \xi(r'), \quad (3)$$

where $\phi(s_i)$ is the selection function at distance s_i from the origin and J_3 is the mean number of excess galaxies out to a distance r around each galaxy. Even though in the last scheme the weights depend on the unknown correlation function, in practice, it is not very sensitive to the exact form of $\xi(r)$ (e.g., Loveday et al. 1992; Marzke, Huchra & Geller 1994). In this work we adopt the minimum-variance weighting and take $J_3(r = 30 h^{-1} \text{ Mpc}) \sim 1100$, obtained by using the real-space correlation function of Davis & Peebles (1983). The mean densities were calculated using the estimator

$$\bar{n} = \sum_{i=1}^{N_{gal}} w_i / \int_{s_{min}}^{s_{max}} dV \phi(s) w(s) \quad (4)$$

where again $\phi(s)$ is the selection function, derived from the luminosity function and $w(s)$ is the weight (e.g., Davis & Huchra 1982). The errors for the redshift space correlation function ($\xi(s)$) as well as for the real-space correlation discussed below, were calculated by means of bootstrap resampling (Ling, Frenk & Barrow 1986). For the volume-limited samples the total of bootstraps was 50, while for magnitude-limited samples 25 resamplings were calculated. As shown by Fisher et al. (1994), bootstrapping tends to overestimate the true errors, so that the estimate of the latter will in general be rather conservative.

3.2. Real space

In order to estimate real space correlation functions, we follow Davis & Peebles (1983). For any two galaxies with redshifts \mathbf{s}_1 and \mathbf{s}_2 , we define the separation in redshift space, and the

separation perpendicular to the line of sight respectively as

$$\mathbf{s} = \mathbf{s}_1 - \mathbf{s}_2, \quad \mathbf{l} = \frac{1}{2}(\mathbf{s}_1 + \mathbf{s}_2), \quad (5)$$

in the small angle approximation. From these parameters one can derive π , the separation between two galaxies parallel to the line of sight and r_p , the separation perpendicular to the line of sight using:

$$\pi = \frac{\mathbf{s} \cdot \mathbf{l}}{|\mathbf{l}|}, \quad r_p = \sqrt{|\mathbf{s}|^2 - \pi^2}. \quad (6)$$

These are then used to compute the statistic $\xi(r_p, \pi)$ estimated from the pair-counts as

$$1 + \xi(r_p, \pi) = \frac{DD(r_p, \pi)RR(r_p, \pi)}{[DR(r_p, \pi)]^2}. \quad (7)$$

From $\xi(r_p, \pi)$ we define the projected function:

$$\omega(r_p) = 2 \int_0^\infty d\pi \quad \xi(r_p, \pi), \quad (8)$$

which is related to the real space correlation function through

$$\omega(r_p) = 2 \int_0^\infty dy \quad \xi[(r_p^2 + y^2)^{1/2}]. \quad (9)$$

The inverse is the Abel integral:

$$\xi(r) = -\frac{1}{\pi} \int_r^\infty dr_p \frac{\omega'(r_p)}{(r_p^2 - r^2)^{1/2}}, \quad (10)$$

where $\omega'(r_p)$ is the first derivative of $\omega(r_p)$. If the real space correlation function is a power-law, the integral for $\omega(r_p)$ can be performed analytically to give

$$\omega(r_p) = r_p \left(\frac{r_0}{r_p}\right)^\gamma \frac{\Gamma(\frac{1}{2})\Gamma(\frac{\gamma-1}{2})}{\Gamma(\frac{\gamma}{2})}. \quad (11)$$

3.3. Biasing

The variance of galaxy counts measures the clustering amplitude at intermediate scales. It is also a useful quantity to compare models and data. The variance in the counts is defined as

$$\langle (N - nV)^2 \rangle = nV + n^2 V^2 \sigma^2, \quad (12)$$

where nV is the mean number of galaxies in the volume V and $n^2 V^2 \sigma^2$ is the mean number of galaxies in excess of random inside a sphere of volume V . It is related to the moment of the correlation function (Peebles 1980)

$$\sigma^2 = \frac{1}{V^2} \int_V dV_1 dV_2 \xi(|r_1 - r_2|), \quad (13)$$

which can be calculated numerically. For a power law correlation function $\xi(r) = (r/r_o)^\gamma$, and a spherical volume of radius R we get

$$\sigma^2(R) = 72(r_o/R)^\gamma / [2^\gamma(3 - \gamma)(4 - \gamma)(6 - \gamma)]. \quad (14)$$

This is the expression we have used to compute σ_8 , and which is often used to normalize theoretical models.

The relative bias between two different samples at a given separation s may be estimated through (e.g., Benoist et al. 1996) :

$$\frac{b}{b_*}(s) = \sqrt{\frac{\xi(s)}{\xi_*(s)}} = \sqrt{\frac{J_3(s)}{J_{3*}(s)}}, \quad (15)$$

where the starred symbols denote a sample taken as a fiducial. The relative bias of the clustering may also be estimated through

$$\frac{b}{b_*}(s) = \sqrt{\frac{\sigma^2(s)}{\sigma_*^2(s)}}, \quad (16)$$

where σ^2 is the variance of counts in cells described above.

These are the expressions used in this work to calculate the relative bias between galaxies of different luminosities relative to L^* galaxies, as well as for different morphological types and colors.

4. Magnitude-limited Samples

In order to estimate the effects due to the finite volume we are probing and to estimate the importance of cosmic variance, we compare the clustering properties of the individual SSRS2 south and north samples as well as the combined sample, with previous estimates of ξ . In this analysis, we have computed $\xi(s)$ taking into account all galaxies brighter than $M = -13$ in the velocity range $500 < v < 12,000 \text{ kms}^{-1}$. The correlation function was computed using the minimum-variance weighting discussed in Section 3 and a random background catalog of 10,000 points for the individual samples and 20,000 points for the combined sample. In the calculation of the selection function we have used the Schechter parameters determined for the entire SSRS2 survey by da Costa et al. (1997), which are $M^* = -19.55$ and $\alpha = -1.15$. These values are virtually identical to those measured by da Costa et al. (1994) for the SSRS2 south.

We tested whether our results are affected by the presence of clusters of galaxies. For this we used a list of galaxy clusters with richness $R \geq 1$ (J. Huchra, private communication). All galaxies whose positions were within one Abell radius of the central position of cluster, and that had radial velocities within 500 kms^{-1} of the cluster's mean radial velocity were culled from the sample. We find that the correlation parameters are virtually unchanged for the vast majority of the samples,

and when there are changes, these are within the quoted errors of the complete sample. Therefore, we will not consider the removal of galaxies in clusters in this work.

The redshift space correlation function, $\xi(s)$, for the SSRS2 samples is shown in Fig. 1, where we plot the correlation function out to separations of $30 h^{-1}$ Mpc. For the sake of clarity, in the figure we only show error bars calculated for the combined sample. One can see that beyond $\sim 15 h^{-1}$ Mpc, the errors become progressively larger, and sometimes the sample-to-sample variations are larger than the estimated errors. In general, $\xi(s)$ is adequately described by a power-law on small scales. For most cases in this paper, the power-law fits were calculated in the interval $2 < s < 11 h^{-1}$ Mpc. The upper-limit was chosen because there is a suggestion of an abrupt change of slope in $\xi(s)$ on scales $s \lesssim 12 h^{-1}$ Mpc. The lower-limit was chosen to minimize the effects on $\xi(s)$ due to peculiar motions of galaxies in virialized systems. The best power-law fits obtained for each sub-sample of the SSRS2 are represented as lines in Fig. 1, as explained in the caption. The correlation parameters derived from the fits are presented in Table 1, where we list: the sample identification (column 1); the correlation length (column 2) and slope γ_s (column 3) obtained from the power-law fits; and in column (4) the rms variance in galaxy counts within spheres $8 h^{-1}$ Mpc in radius, followed in columns (5) through (7) by the same parameters determined for real space, which will be discussed below.

An inspection of both Table 1 and Fig. 1 shows that the redshift correlation functions for SSRS2 sub-samples are very similar on small scales ($s < 10 h^{-1}$ Mpc). This also demonstrates that the sampling variations are consistent with the error estimates, at least in the range of separations for which the fits are calculated. In Fig. 2 we compare $\xi(s)$ measured in this work for the combined SSRS2 with the $\xi(s)$ measured in other surveys - the sparsely sampled Stromlo-APM survey (Loveday et al. 1995), the Las Campanas Redshift Survey (LCRS) (Tucker et al. 1997), and that measured by Fisher et al. (1994) for the 1.2 Jy *IRAS* survey. The fit parameters calculated in these papers, as well as by other workers can be found in Table 2. Despite small differences in amplitude, the shapes of the three optical surveys are remarkably similar. It is important to note that the volumes of the Stromlo-APM ($2.5 \times 10^6 h^{-3} \text{ Mpc}^3$) and the LCRS ($2.6 \times 10^6 h^{-3} \text{ Mpc}^3$) are about 5 times larger than that of the SSRS2 ($5.2 \times 10^5 h^{-3} \text{ Mpc}^3$), and probe different regions of space, and thus independent structures. The lower amplitude of the *IRAS* survey compared to the optical samples reflects the relative bias that exists between optically and infrared-selected galaxies, which will be further discussed in Section 6 below.

In Fig. 3, we compare our power-law fit parameters with equivalent measurements by other authors (see Table 2). In general, there is a good agreement between our values for the redshift space parameters and those obtained from other optical surveys, specially the Stromlo-APM and LCRS.

The effect of redshift distortions on the observed redshift correlation function has also been estimated for the SSRS2. These distortions are caused by the peculiar velocities of galaxies, which on large scales, are due to the infall of galaxies from low-density regions into high-density regions,

while on small scales the correlations are smeared out by virial motions of galaxies in groups and clusters (e.g., Kaiser 1987). As described in Section 3, these effects may be accounted for by calculating the correlation function as a function of the separations parallel and perpendicular to the line of sight, which can then be used to define the $\omega(r_p)$ estimator, which is unaffected by redshift distortions. However, one should bear in mind that in general the calculation of the real space correlation function is much more susceptible to noise than that calculated in redshift space.

From the correlation functions $\xi(r_p, \pi)$ computed using the minimum-variance weighting scheme, we have obtained $\omega(r_p)$. From power-law fits, in the interval $2 < r_p < 10 h^{-1}$ Mpc, we have derived the correlation parameters listed in Table 1. By comparing the real space fit parameters obtained in this work (Table 1) with previous measures (columns 4 and 5 in Table 2), we find a good agreement with the real space measurements of Davis & Peebles (1983), Loveday et al. (1995) and Marzke et al. (1995).

The fit to the real space correlation function for the combined sample is compared in Fig. 4 with the redshift space correlation function. One can see that at intermediate separations the redshift $\xi(s)$ is amplified relative to the real space correlation $\xi(r)$. The small amplification suggests that the observed redshift distribution is close to the real space distribution. At separations of $\sim 10 h^{-1}$ Mpc, the ratio between the real and redshift space correlations is ~ 1.5 . In the linear regime, peculiar motions on large scales cause $\xi(r)$ to be amplified by a factor $\sim 1 + \frac{1}{2}\beta + \frac{1}{5}\beta^2$ where $\beta = \frac{\Omega^{0.6}}{b}$ and b is the linear biasing factor (Kaiser 1987). Therefore, a rough estimate for β is ~ 0.6 , on scales of the order of $10 h^{-1}$ Mpc, consistent with that determined by Loveday et al. (1996).

5. The Clustering Dependence on the Internal Properties of Galaxies

5.1. Luminosity

In this work we use the combined SSRS2, as well as the SSRS2 north and south sub-samples to further explore the clustering dependence on luminosity, as was carried out by Benoist et al. (1996), but who only used the SSRS2 south. Probing independent structures in different volumes we can estimate the impact of cosmic variance. It should also be noted that the absolute magnitude limits considered in this section differ slightly from those of Benoist et al. (1996), and were chosen to compare our results with the volume-limited samples of Fisher et al. (1994), which will be discussed in Section 6 below.

The volume-limited samples considered in this section only contain galaxies bright enough that would allow them to be included in the sample when placed at the cutoff distance. We defined samples limited at radial distances of 60, 80, 100 and 120 h^{-1} Mpc. The absolute magnitude limits corresponding to these distances are -18.39, -19.01 (both $L < L^*$), -19.50 ($\sim L^*$) and -19.89 ($L > L^*$), respectively. For all galaxies in these samples, the weighting function is $w(r) = 1$ and

the volume densities are simply the total number of galaxies divided by the corresponding volume.

The correlation functions obtained for the volume-limited sub-samples at the different depths are shown in Fig. 5 for $s \leq 20 h^{-1}$ Mpc, where the different symbols represent different volume limits. For reasons of clarity, we only present error bars for the samples volume-limited at $60 h^{-1}$ and $120 h^{-1}$ Mpc. The meaning of these symbols, as well as the indication of the parent sample (SSRS2 south, north or combined) are shown in each panel. The power-law fits are represented by lines in the figure and the parameters are summarized in Table 3 where we list: in column (1) the sample; in column (2) the depth R ; in column (3) the number of galaxies N_g ; in column (4) the mean density; in columns (5) and (6) the power-law fit parameters and formal errors; and in column (7) σ_8 , the rms fluctuation of the number of galaxies in a sphere of radius $8h^{-1}$ Mpc. The interval used in the fits is $2 < s < 11 h^{-1}$ Mpc, the same as that adopted in the previous section.

An inspection of Table 3 and Fig. 5 shows that the amplitude of $\xi(s)$ tends to increase with the sample depth, the variation being somewhat larger in the northern and combined samples. We point out that $\xi(s)$ for the SSRS2 north (panel b), is noisier because of the smaller number of galaxies, in most cases about half of those in the southern sample. The correlation length (s_0) ranges from $3.8 h^{-1}$ Mpc to $6.8 h^{-1}$ Mpc. However, the slope varies considerably from sample to sample, though with a tendency of becoming steeper as the depth increases.

In order to evaluate the cosmic variance, we show in Fig. 6 $\xi(s)$ for each of the volume-limited sub-samples, but now plotting the results for the southern, northern and combined samples in each panel. For the samples in smaller volumes, the differences between the northern and southern samples are larger than the estimated error calculated for the combined sample, and probably reflect the amplitude of the sample to sample variation, with the north being systematically lower. For the larger volumes the samples present similar behavior, and the variations are generally consistent with the estimated errors.

To remove the effects of distortions due to motions, which may affect our estimates of the strength of clustering and the relative bias between different samples, we have also computed the real-space correlation function for the volume-limited samples. As above, we have computed $\xi(r_p, \pi)$ for the sub-samples volume-limited at $R = 60, 80, 100$ and $120 h^{-1}$ Mpc in each galactic hemisphere and for the combined sample. The resulting real space correlation parameters are listed in Table 4.

In Fig. 7 we compare $\xi(s)$ measured for each volume limit, denoted by open symbols, with the real-space correlation fits described above, represented as a solid line. For the sake of clarity, we only show the fits we measure for the combined sample, as this will be the one less affected by noise. The smearing due to motions in virialized systems for $r < 3 h^{-1}$ Mpc is quite noticeable for all samples, while the effect of peculiar motions is only obvious for the smaller volumes, little evidence being seen in the samples in larger volumes.

The dependence of clustering in redshift-space (as measured by σ_8) with luminosity (as measured by the limiting absolute magnitude of each sample) is shown in Fig. 8(a), where we

use as fiducial magnitude the value of $M^*=-19.55$ (see Section 4). The figure shows an overall behavior consistent with that found by Benoist et al. (1996) and which is detected in all samples, further demonstrating that this effect is unlikely to be spurious. This result supports their finding that there is a dependence of clustering on luminosity, as measured in redshift space. To further investigate its reality, we have computed $\xi(r)$ in real space for the same volume limited samples. The results are shown in Fig. 8(b). Here again it is immediately apparent that the clustering amplitude increases with luminosity in the same way as seen in redshift space. On the whole, these results, using a larger sample, confirm in real space the conclusions of Benoist et al. (1996).

In Fig. 9 we present the relative bias with scale calculated using equation (15), where we compare the the correlation function for the volume-limited samples at 60, 80 and 120 h^{-1} Mpc relative to the 100 h^{-1} Mpc sample. From the figure one may see that there are only minor differences between the smaller volumes. In the case of the sample volume-limited at 120 h^{-1} Mpc, the relative bias is fairly constant over the range of scales we consider at ~ 1.5 . This suggests that the luminosity bias is scale-independent, and that it starts to become important only for galaxies brighter than $\sim L^*$.

5.2. Morphology

Since all galaxies in the SSRS2 have morphological classifications we can also analyze the clustering dependence on morphology. With this aim, we have calculated $\xi(s)$ and $\xi(r)$ for the SSRS2 for different morphological types, dividing galaxies into broad morphological bins - early types comprising E, S0 and S0-a, and late types containing Sa galaxies and later. In contrast to the results of the Stromlo-APM, the luminosity function parameters used in the selection function for both samples are quite similar to those measured for the SSRS2 as a whole (Marzke et al. 1997). Furthermore, since sample-to-sample variations are within our estimated errors both for the magnitude and volume-limited samples, as shown in Section 4, in the analysis below we only consider the combined sample to improve the statistics.

The resulting correlation functions for early and late type galaxies are presented in Figure 10 panel (a) in redshift space and (b) in real space, while the fit parameters are presented in Table 5. For the late type galaxies we find that the correlation function is adequately described by ($s_0 = 5.4 \pm 0.2 h^{-1}$ Mpc; $\gamma_s = 1.48 \pm 0.09$), while for early types we find $s_0 = 6.5 \pm 0.2 h^{-1}$ Mpc; $\gamma_s = 1.86 \pm 0.11$. Our values for early type galaxies are close to those of Santiago & da Costa for the diameter-limited SSRS ($s_0 = 6.0 \pm 1.5 h^{-1}$ Mpc, $\gamma_s = 1.69$) and Hermit et al. (1996) for the ORS, who measure $s_0 = 6.7$ and $\gamma_s = 1.52$. Our value for late types is somewhat larger than that measured by Santiago & da Costa (1990), while a proper comparison with Hermit et al. (1996) cannot be made, because we have not subdivided spirals into earlier (Sa/Sb) and later (Sc/Sd) types as they did. A comparison between the fit parameters obtained from available redshift space correlation functions, is shown in Fig. 11, where open symbols represent fits for late type galaxies and solid symbols represent early types. Although all works agree that early types are more clustered than

late types, as indicated by the larger correlation length, the scatter is large with the Stromlo-APM results yielding very extreme results. This, in turn, implies large uncertainties in the measurement of the relative bias between the two populations. Based on the redshift space information, we estimate the relative bias between morphological types as 1.25.

However, for a proper estimate of the dependence of the correlation properties on morphology it is important to take into account the fact that redshift distortions may affect early and late type galaxies in different ways. Therefore a more meaningful comparison must be carried out in real space. The values we measure for the correlation length in real space for early types ($r_0=6.0\pm 0.4$; $\gamma_r=1.91\pm 0.18$) show a very good agreement with those of Loveday et al. (1995), ($r_0=5.9\pm 0.7$; $\gamma_r=1.85\pm 0.13$). For late types we find ($r_0=5.3\pm 0.3$; $\gamma_r=1.89\pm 0.15$), which is somewhat larger than those measured by the same authors ($r_0=4.4\pm 0.1$; $\gamma_r=1.64\pm 0.05$).

Our value of the correlation length is significantly smaller than that measured by Guzzo et al. (1997) ($r_0=8.4\pm 0.8$; $\gamma_r=2.05\pm 0.09$) for early types. We should note that their sample is volume-limited at $M < -19.5$, whereas we consider galaxies down to $M = -13$. In order to compare with these authors we consider a volume-limited sub-sample of SSRS2 galaxies with $M \leq -19.5$, which corresponds to maximum distance of $100 h^{-1}$ Mpc. Using this sample, for early types we measure ($r_0=5.7\pm 0.8$; $\gamma_r=2.09\pm 0.49$) while for late types we find ($r_0=5.0\pm 0.5$; $\gamma_r=2.01\pm 0.28$). For both early as well as late types, there are still discrepancies relative to the results of Guzzo et al. (1997), which could reflect the paucity of rich clusters in our sample.

By using the variance, we estimate that the relative bias between the different morphologies is $b_{E+S0}/b_S = 1.18\pm 0.15$ in a sample where clusters are not important. This value is smaller than the determination derived from the real-space correlations of Loveday et al. (1995) $b_{E+S0}/b_S = 1.33$ and Guzzo et al. (1997) $b_{E+S0}/b_S = 1.68$. From these results we may conclude that the relative bias between the two populations range from roughly 1.2 to 1.7, depending on the cluster abundance in the sample, with the former value representing a lower limit.

We have also calculated the correlation function for galaxies discriminated by morphological types for volume-limited samples using the same absolute magnitude limits as in Section 5.1. This calculation was carried out both in redshift, as well as real space, and the results are presented in Tables 6 and 7 respectively. In redshift space there is a trend of the correlation function amplitude increasing with luminosity for both morphological classes. The magnitude of this variation is larger for early types than for late types, although the errors are large. The same trend may be inferred from the analysis in real space, as shown in Figure 12(a), where we compare the σ_8 values obtained for the different sub-samples. Here it may be clearly seen that there is a trend of σ_8 increasing with luminosity, suggesting that the morphological and luminosity segregations are two separate effects.

Using equation (15) we can also examine how the relative bias varies as a function of scale. This is shown in Figure 12(b), using the real space correlation functions. In contrast to the luminosity bias we find that the morphological bias presents a small decrease from ~ 1.4 on small

scales to ~ 1.0 on larger scales ($\sim 8 h^{-1}$ Mpc). Although the latter value is slightly smaller than that estimated through the σ_8 values ($b_{E+S_0}/b_S = 1.18 \pm 0.15$), it is still within the estimated error. A similar behavior of the morphological bias changing with scale, was found by Hermit et al. (1996) but using the redshift space correlation function of the ORS, which may not be as meaningful, because of possible biases introduced by virial motions.

Taken together, the above results are consistent with the interpretation that luminosity segregation could be a primordial effect, while the morphological segregation could be enhanced by environmental effects (e.g. Loveday et al. 1995).

5.3. Colors

Another internal characteristic available in the present catalog is color. Although morphology and colors are correlated the scatter is large, and galaxies of a given type exhibit a broad range of colors, indicating different star-formation histories. On the other hand, colors are easily measured and are an objective criterion, in particular for samples of distant galaxies, whereas the morphological classification is somewhat subjective and becomes increasingly difficult to carry out as the apparent sizes of galaxies get smaller. A further evidence that morphology and colors have somewhat different distributions comes from the calculation of the luminosity function, which presents significantly different shapes for blue and red galaxies (Marzke & da Costa 1997), while the luminosity function calculated by separating galaxies between early and late types presents similar Schechter parameters (Marzke et al. 1997).

The few works calculating the correlation properties of galaxies divided by colors present rather conflicting results for the deep samples. Works by Infante & Pritchett (1993) and Landy, Szalay & Koo (1996) using the angular correlation function show that the correlation of redder galaxies is significantly stronger than for bluer galaxies, except for the very bluest ones (Landy et al. 1996). Carlberg et al. (1996) analyzing a redshift survey of K-band selected galaxies, find that for $0.3 \leq z \leq 0.9$ red galaxies are more correlated than blue galaxies by a factor of five. These results differ from those of Le Fèvre et al. (1996) who find that at $z \geq 0.5$ blue and red galaxies have the same correlation properties, while for $0.2 \leq z \leq 0.5$ blue galaxies are less correlated than red ones. For nearby galaxies, Tucker et al. (1996) have calculated the correlation function and showed that at small scales ($s \leq 10 h^{-1}$ Mpc) red galaxies ($[b_J - R]_0 > 1.25$) cluster more strongly than blue ($[b_J - R]_0 < 1.05$) ones, while for larger scales no evidence of color segregation is seen.

In order to make an independent estimation of the dependence of $\xi(s)$ on colors, we use the the $m_B = 14.5$ sample described in Section 2, which contains galaxies in both galactic hemispheres. As mentioned in Section 2, this bright limit was used because of incompleteness in colors, as we are restricted to galaxies with measurements in the Lauberts & Valentijn (1989) catalog. In this work we adopted the restframe color cutoff as $(B_T - R_T)_0 = 1.3$ which is roughly the color of an Sbc galaxy, and was the criterion adopted by Marzke & da Costa (1997) in the determination of the

luminosity function by colors. This value is close to the median value of $B_T - R_T$ in our sample which is $B_T - R_T = 1.2$. The conversion of observed into restframe colors used the no-evolution models calculated by Bruzual & Charlot (1993), where we assume that the B and R measures in the Lauberts & Valentijn (1989) catalog are on the same system of b_J and r_F used by Bruzual & Charlot (1993). To calculate $\xi(s)$ we used the following Schechter function parameters; for blue galaxies ($B_T - R_T \leq 1.3$), $M^* = -19.43$, $\alpha = -1.46$; for red galaxies ($B_T - R_T > 1.3$), $M^* = -19.25$, $\alpha = -0.73$, which were obtained by Marzke & da Costa (1997). The sample, which only considers galaxies out to a maximum distance of 8000 kms^{-1} , contains 387 blue and 219 red galaxies.

The results of the two-point correlation function are shown in Figure 13 (a) for redshift space while the fit parameters may be found in Table 8. Because of the small number of objects, the correlation function is very noisy, yet it is unquestionable that the red galaxies present a systematically higher amplitude at all separations compared to blue galaxies. In order to verify how sensitive the results may be to incompleteness, we re-calculated $\xi(s)$ for the $m_B = 14.2$ sample which is 92 % complete in colors. The fit parameters present a similar behavior, although the values differ from those measured for the 14.5 sample. The results we obtain for the samples discriminated in colors present a qualitative agreement with those of Tucker et al. (1996), in the sense that red galaxies are more strongly correlated than blue galaxies.

We have also calculated the real-space correlation function for the 14.5 sample and the power-law fit is presented in Fig. 13 (b), together with the redshift space correlation. The figure shows that the slopes of both power law fits are fairly similar ($\gamma_r = 1.99$ for blue, $\gamma_r = 2.18$ for red galaxies), though the uncertainties are rather large, in particular for the red galaxies. The observed $\xi(r)$ suggests that red galaxies are probably more affected by peculiar motions than blue galaxies. Because of the relatively small size of the sample with colors, we have not been able to investigate the dependence on luminosity, which would be dominated by errors because of the small number of objects assigned to each luminosity bin.

The relative bias estimated from σ_8 in real space is $b_R/b_B = 1.40 \pm 0.33$, and a similar result is obtained if the redshift space results are considered. As in the case of luminosity and morphology, one may calculate the relative bias between galaxies of different colors as a function of scale, which is presented in Fig. 14. Because the observed correlation function is rather noisy, for this plot we used the fits to $\xi(r)$. Taking the results at face value they would suggest that the relative bias between red and blue galaxies on small scales is comparable to that seen for early and late type galaxies. However, it levels off more rapidly ($\sim 4 h^{-1} \text{ Mpc}$), remaining constant at $b_R/b_B \sim 1.2$ thereafter. This behavior could be the result of evolution due to environmental effects, where early type galaxies in higher density regions lost their gas more rapidly than bluer galaxies, and thus present a much lower star formation rate. However, because the errors are large, these results should only be considered as tentative.

6. Comparison with *IRAS* galaxies

In this section we compare the correlation properties of both the entire SSRS2 sample as well as for the volume-limited sub-samples described in Section 5.1 with the *IRAS* 1.2 Jy survey (Fisher et al. 1994). In Fig. 2 we presented a comparison between $\xi(s)$ as measured by different surveys. In that figure it is quite apparent that the three optical surveys are in very good agreement, while the *IRAS* survey presents systematically lower amplitude, which reflects the bias that exists between the distribution of optically-selected and infrared-selected galaxies, previously noted by several authors (Davis et al 1988; Babul & Postman 1990; Lahav et al. 1990; Saunders et al. 1992; Strauss et al. 1992; Fisher et al. 1994).

The clustering dependence on infrared luminosity was investigated by Fisher et al. (1994), using different sub-samples of the *IRAS* 1.2 Jy survey, who found no evidence for such dependence. This result differs from that presented in Section 5.1 above, and a comparison between the different volume-limited sub-samples of SSRS2 and *IRAS* galaxies is presented in Fig. 15. We point out that as there are no available measures in real space calculated by Fisher et al. (1994), here we use the values obtained in redshift space, which are presented in the last column of Table 3. The inspection of this figure shows that the amplitude and shape of $\xi(s)$ have the best agreement for the $60 h^{-1}$ Mpc sample ($M < -18.39$), while the other SSRS2 sub-samples containing brighter galaxies present $\xi(s)_{SSRS2} > \xi(s)_{IRAS}$. A possible explanation for the different behavior of the optical and *IRAS* relative to luminosity is that the optical luminosity is more strongly related to the mass, while the infrared luminosity of *IRAS* galaxies reflects rather the star-formation rate which is only weakly dependent on the mass (Davis et al. 1988).

The relative bias between the different volume-limited samples of the SSRS2 and the *IRAS* 1.2 Jy survey are shown in Fig. 16(a). For this calculation we used the variance calculated in redshift space, shown in column (7) of Table 3, with the values in Table 1 of Fisher et al. (1994). An inspection of the figure shows that the relative bias between both samples increases with luminosity, ranging from $b_o/b_I = 0.94$ to $b_o/b_I=1.91$. The smallest value is obtained for the sample which includes less luminous galaxies ($M < -18.39$), while the largest value is for the sample with the brightest galaxies ($M < -19.89$). This result suggests that the relative bias between optical and *IRAS* galaxies depends on the luminosity of the objects, the less luminous optical galaxies showing a clustering amplitude comparable to that found for *IRAS* galaxies.

The mean relative bias between the optical and *IRAS* samples may be estimated using the σ_8 values both in redshift and real space. For this we use the σ_8 for the magnitude-limited SSRS2 sample and the 1.2 Jy *IRAS* sample (Fisher et al. 1994), using for the former, values in the last column of Table 1. By using the value of σ_8 for the combined sample we find that the relative bias between optical and *IRAS* sample is $\sim 1.20 \pm 0.07$.

The bias in real space can be obtained using the σ_8 value derived from the real space correlation function. For our combined sample we measure $\sigma_8 = 0.96 \pm 0.06$, while Fisher et al. (1994) quote for *IRAS* galaxies $\sigma_8 = 0.69 \pm 0.04$. This result implies in a relative bias

$b_o/b_i = 1.39 \pm 0.17$, $\sim 17\%$ larger than that estimated in redshift space. This value is consistent with the value of $\sigma_8 = 1.38 \pm 0.12$ reported by Fisher et al. (1994).

One may also calculate the relative bias with scale in real space by using equation (15) for the combined magnitude-limited optical and flux-limited *IRAS* samples. The results are presented in Fig. 16(b). Notwithstanding the large error bars, the results suggest that relative bias between optical and *IRAS* galaxies decrease with scale varying from about 1.4 on $1 h^{-1}$ Mpc to close to 1 on $10 h^{-1}$ Mpc scales (e.g. Strauss et al. 1992).

7. Summary

We have investigated the correlation properties of galaxies in the SSRS2 catalog for which we have considered both volume and magnitude-limited samples. The main results may be summarized as follows:

- In spite of the small volume probed relative to the scale of inhomogeneities, we find an excellent agreement between our correlation function and those of other surveys probing volumes more than 5 times larger. This result is in contradiction with the fractal interpretation of the galaxy distribution in the Universe, which predicts that the correlation length increases with volume.
- The relatively small differences between redshift and real space correlations on intermediate scales ($s \sim 10 h^{-1}$ Mpc) suggest a low value of $\beta = \Omega^{0.6}/b < 1$, indicating that the redshift distribution of galaxies is close to that in real space.
- We confirm the existence of a luminosity-dependent bias for super-L* galaxies that is scale-independent, suggesting that it is of primordial nature.
- In contrast, the relative bias between early and late types shows a scale dependence, varying from about 1.4 on small scales to 1 at $\sim 8 h^{-1}$ Mpc. The mean relative bias is found to be $b_{E+S0}/b_S \sim 1.2$. This small value, when compared to previous surveys, probably reflects the paucity of rich clusters in the surveyed region.
- Both early and late types show separately a luminosity-dependent bias similar to the sample as a whole further suggesting that the luminosity bias is primordial in nature while the excess clustering of early types relative to spirals on small scales may be caused by environmental effects.
- The relative bias between red and blue galaxies is similar to that observed between early and late type galaxies. However, it levels off on smaller scales $\sim 4 h^{-1}$ Mpc at a constant value of about 1.2. We find that the mean relative bias of galaxies selected by colors is greater than when selected by morphologies. We point out, however, that color samples are significantly smaller and the uncertainties correspondingly larger.

- The relative bias between optical and IRAS galaxies also varies with scale at least out to $\sim 10 h^{-1}$ Mpc and shows a strong luminosity dependence. The mean relative bias between optical and *IRAS* is $b_o/b_I = 1.39 \pm 0.17$ in real space.

The results presented here offer key elements for constraining galaxy formation models. Although intriguing, we should note that the samples are still relatively small, especially those with color information, so these results should be considered only as tentative. Future larger samples are essential to further investigate these effects, and which are likely to give more insight on the relation between galaxies and large-scale structures, and on the galaxy formation process.

We would like to thank our SSRS2 collaborators for allowing us to use the data in advance of its publication. We also thank K. Fisher and J. Loveday for helpful discussions and for providing us with their results. We thank D. Tucker for providing results of the LCRS survey and S. Hermit for ORS results. We also thank R. Marzke and M. Vogele for many useful discussions. CNAW acknowledges partial support from CNPq grants 301364/86-9, 453488/96-0 and from the ESO Visitor program. PSP acknowledges funding from CNPq grant 301373/86-8 and from the Centro Latino-Americano de Física.

REFERENCES

- Alonso, M. V., da Costa, L. N., Latham, D. W., Pellegrini, P. S., & Milone, A. E. 1994, *AJ*, 108, 1987
- Babul, A., & Postman, M. 1990, *ApJ*, 359, 280
- Benoist, C., Maurogordato, S., da Costa, L. N., Cappi, A., & Schaeffer, R. 1996, *ApJ* 472, 452
- Bruzual, A. G., & Charlot, S. 1993, *ApJ*, 405, 538
- Carlberg, R.G., Cowie, L. L., Songaila, A., & Hu, E. M. 1996, *ApJ*, 484, 538
- da Costa, L. N., Geller, M. J., Pellegrini, P. S., Latham, D. W., Fairall, A. P., Marzke, R. O., Willmer, C. N. A., Huchra, J. P., Calderon, J. H., Ramella, M. & Kurtz, M. J. 1994, *ApJ*, 424, L1
- da Costa, L. N., et al. 1997, in preparation
- Davis, M., & Geller, M. J. 1976, *ApJ*, 208, 13
- Davis, M., & Huchra, J. P. 1982, *ApJ*, 254, 437
- Davis, M., & Peebles, P. J. E. 1983, *ApJ*, 267, 465
- Davis, M., Meiksin, A., Strauss, M., da Costa, L. N. & Yahil, A. 1988, *ApJ*, 333, L9
- de Lapparent, V., Geller, M. J. & Huchra, J. P. 1988, *ApJ*, 332, 44
- Fisher, K. B., Davis, M., Strauss, M. A., Yahil, A. & Huchra, J. P. 1994, *MNRAS*, 266,50
- Geller, M. J., & Huchra, J. P., 1989, *Science*, 246, 897
- Giovanelli, R., Haynes, M. P., & Chincarini, G. 1986, *ApJ*, 300, 77
- Guzzo, L., Strauss, M. A., Fisher, K. B., Giovanelli, R., & Haynes, M. P. 1997, *ApJ*, 489, 37
- Hamilton, A. J. S., 1993, *ApJ*, 417, 19
- Hermit, S., Santiago, B. X., Lahav, O., Strauss, M. A., Davis, M., Dressler, A., & Huchra, J. P. 1996, *MNRAS* 283, 709
- Infante, L., & Pritchett, C. J. 1993, *ApJ*, 439, 565
- Iovino, A., Giovanelli, R., Haynes, M. P., Chincarini, G. & Guzzo, L. 1993, *MNRAS*, 265, 21
- Kaiser, N, 1987, *MNRAS*, 227, 1
- Lahav, O., Nemiroff, R., Piran, T. 1990, *ApJ*, 350, 119
- Landy, S. D., Szalay, A. S., & Koo, D. C. 1996, *ApJ*, 460, 94
- Lasker, B. M., Sturch, C. R., McLean, B. M., Russel, J. L., Jenker, H., & Shara, M. 1990, *AJ*, 99, 2019 (GSC)
- Lauberts, A. 1982, *The ESO/Uppsala Catalogue of the ESO Quick Blue Survey*, (Garching: ESO)
- Lauberts, A., & Valentijn, E. A. 1989, *The Surface Photometry Catalogue of the ESO/Uppsala Survey*,(Garching: ESO)

- Le Fèvre, O., Hudon, D., Lilly, S. J., Crampton, D., Hammer, F., & Tresse, L. 1996, *ApJ*, 461, 534
- Ling, E. N., Frenk, C. S., & Barrow, J. D. 1986, *MNRAS*, 223, 21P
- Loveday, J., Efstathiou, G., Maddox, S. J., & Peterson, B. A. 1996, *ApJ*, 468, 1
- Loveday, J., Peterson, B. A., Efstathiou, G., & Maddox, S. J. 1992, *ApJ*, 390, 338
- Loveday, J., Maddox, S. J., Efstathiou, G., & Peterson, B. A. 1995, *ApJ*, 442, 457
- Marzke, R. O., & da Costa, L. N. 1997, *AJ*, 113, 185
- Marzke, R. O., Huchra, J. P., & Geller, M. J. 1994, *ApJ*, 428, 43
- Marzke, R. O., Geller, M. J., da Costa, L. N., & Huchra, J. P. 1995, *AJ*, 110, 477
- Marzke, R. O., da Costa, L. N., Pellegrini, P. S., & Willmer, C. N. A. 1997, *AJ*, submitted.
- Peebles, P. J. E. 1980, *The Large Scale Structure of the Universe*, (Princeton: Princeton Univ. Press)
- Pellegrini, P. S., da Costa, L. N., Huchra, J. P., Latham, D. W., & Willmer, C. 1990a., *AJ* 99, 751
- Pellegrini, P. S., Willmer, C. N. A., da Costa, L. N., & Santiago, B. X. 1990b, *ApJ*, 350, 95
- Santiago B. X. & da Costa, L. N. 1990, *ApJ* 362, 386
- Saunders, W., Rowan-Robinson, M. & Lawrence, A. 1992, *MNRAS*, 258, 134
- Strauss, M. A., Davis, M., Yahil, A., & Huchra, J. P. 1992, *ApJ*, 385, 421
- Tucker, D. L., Oemler, A. A., Kirshner, R. P., Lin, H., Shectman, S. A., Landy, S. D., & Schechter, P. L. 1996, in “CLustering in the Universe”, ed. C. Balkowski, S. Maurogordato, C. Tao, & J. T. T. Van (Gif-sur-Yvette: Editions Frontieres), p. 39.
- Tucker, D. L., et al. 1997, *MNRAS*, 285, 5
- Valotto, C. A., & Lambas, D. G. 1997, *ApJ*, 481, 594
- Vogeley, M., Park, C., Geller, M. J., Huchra, J. P. & Gott, J. R., 1994, *ApJ*, 420, 525
- White, S. D. M., Tully, R. B., & Davis, M. 1988, *APJ*, 333, L45

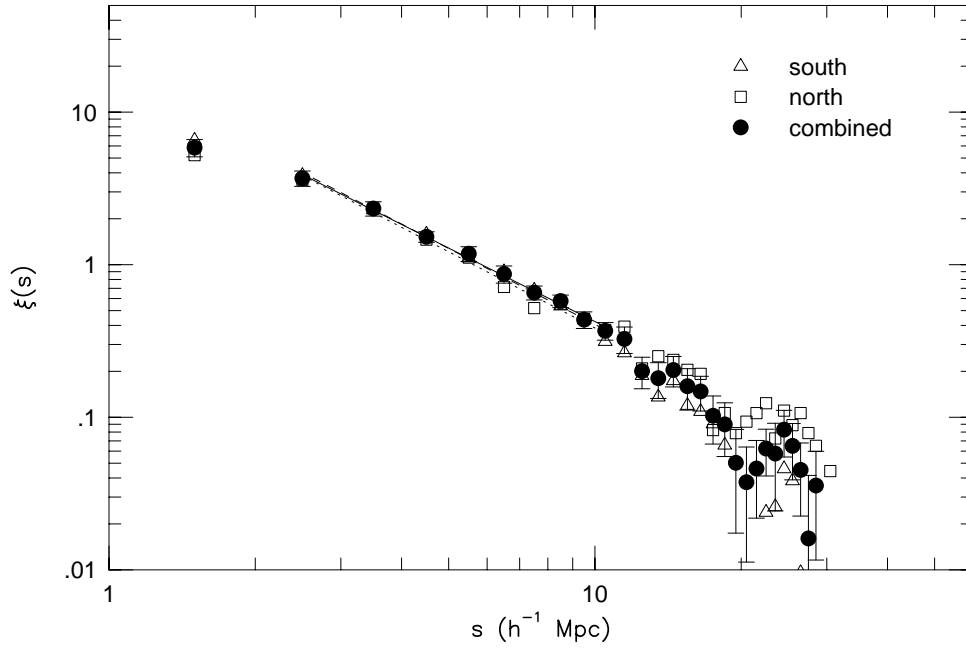


Fig. 1.— Redshift space correlation function using optimal weighting and fits for the southern (open triangles; dashes), northern (open squares; dots) and combined (solid circles; solid line) subsamples of the SSRS2. The fit parameters are presented in Table 1. Error bars, calculated by means of bootstrap resampling are presented only for the combined sample

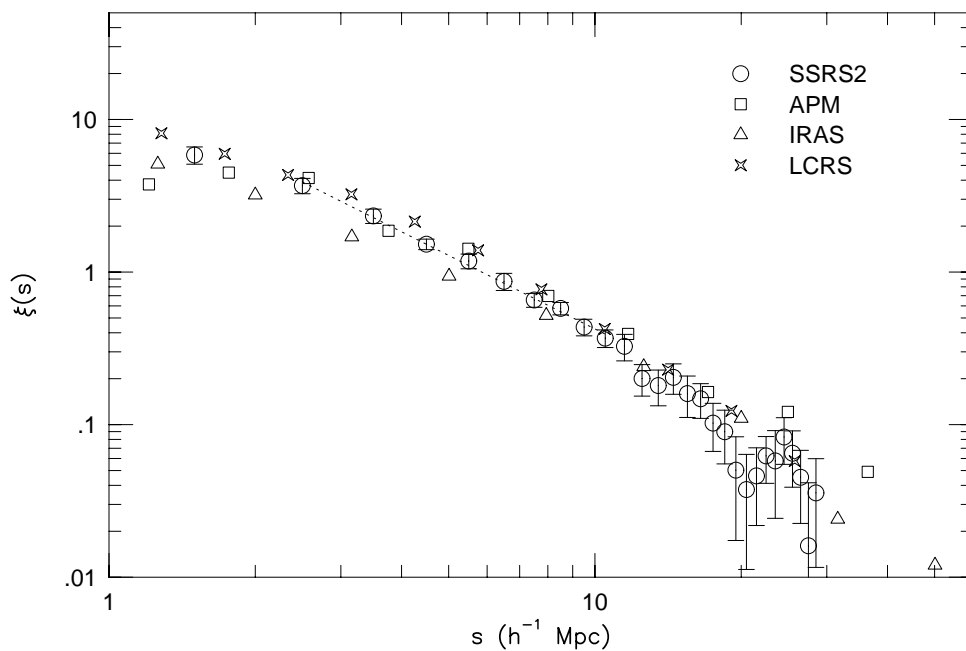


Fig. 2.— Comparison between the redshift correlations of the SSRS2 combined sample (open circles), the optically selected APM (open squares) and LCRS (crosses) and the infrared-selected *IRAS* 1.2Jy (open triangles). The dashed line represents the fit to the SSRS2 correlation function. For the sake of clarity, we only show error bars calculated for the SSRS2 sample.

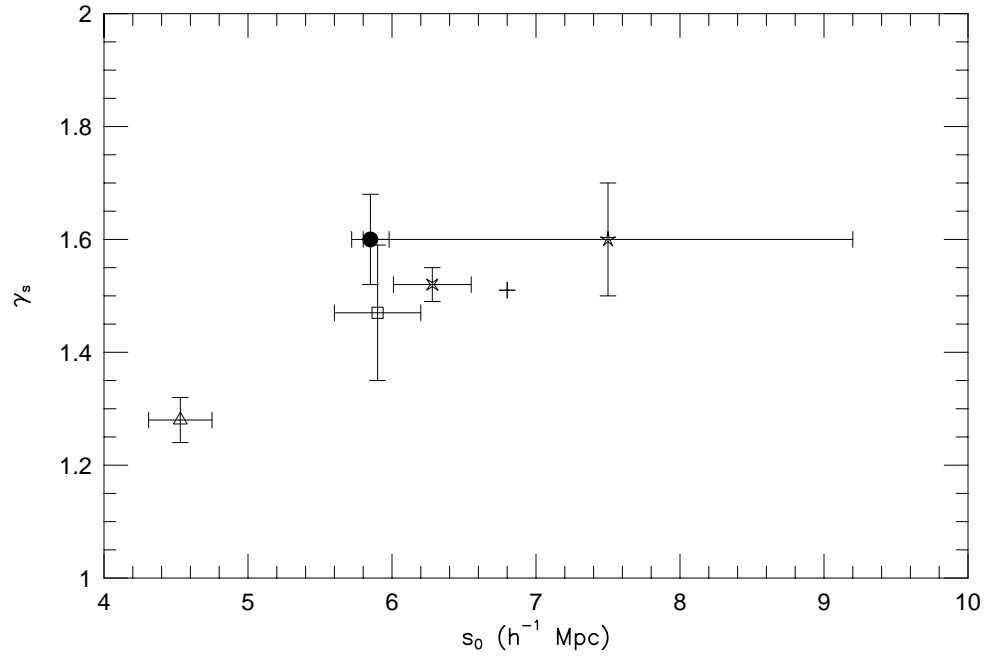


Fig. 3.— Comparison between the correlation function parameters for the SSRS2 combined sample (solid circle), Stromlo-APM (open square), LCRS (cross), *IRAS* 1.2Jy (open triangle), CfA2 (star) and ORS (plus). In the case of this last survey, no error bars were provided.

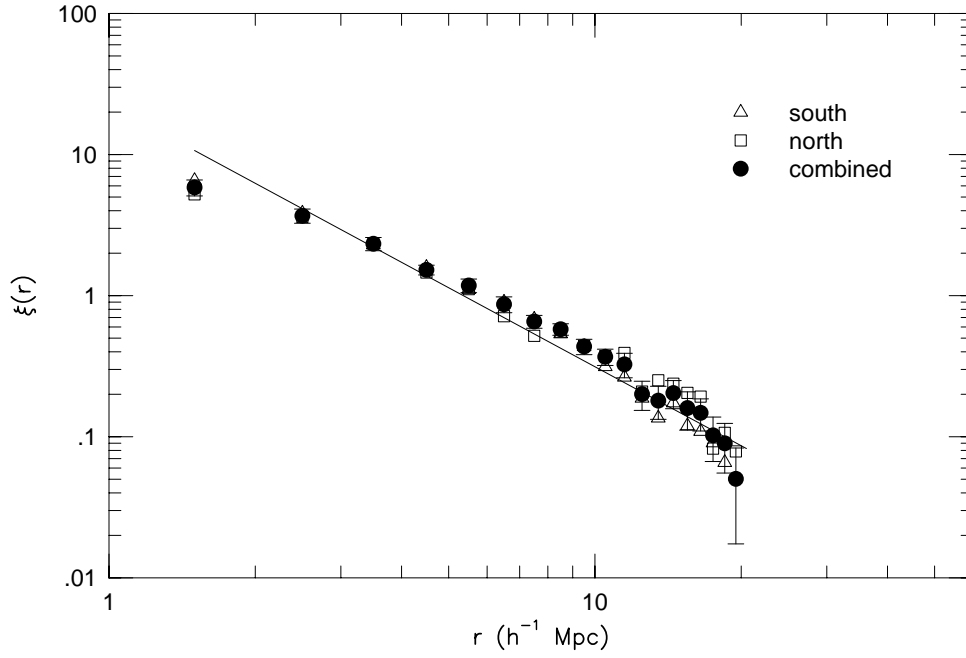


Fig. 4.— Comparison between the real and redshift space correlation functions calculated for the magnitude-limited north and south sub-samples and combined SSRS2. The symbols represent redshift space values (as in Fig. 1), while the solid line represents the real-space fit for combined sample. As in Fig. 1, error bars are only shown for the combined sample.

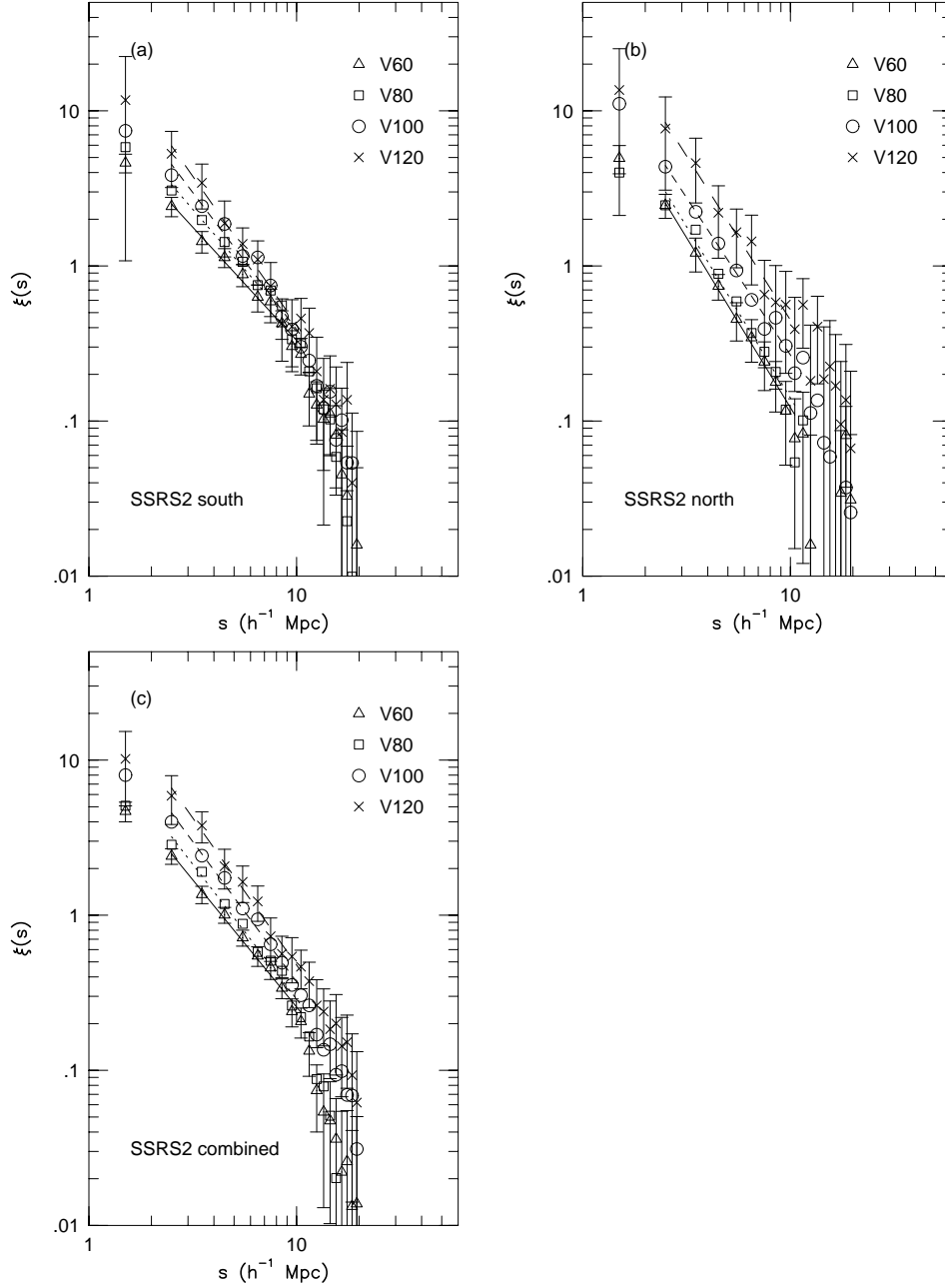


Fig. 5.— Two-point correlation function in redshift space for the (a) southern, (b) northern and (c) combined sub-samples of the SSRS2. The symbols and lines represent the correlation function and fits for the volume-limited sample: at $60 h^{-1}$ Mpc (open triangles, solid line); $80 h^{-1}$ Mpc (open square, dotted line); $100 h^{-1}$ Mpc (open circles, short-dashes) and $120 h^{-1}$ Mpc (crosses, long dashes). The fit parameters can be found in Table 3. The bootstrap error estimates are only shown for the $60 h^{-1}$ Mpc and $120 h^{-1}$ Mpc samples for the sake of clarity.

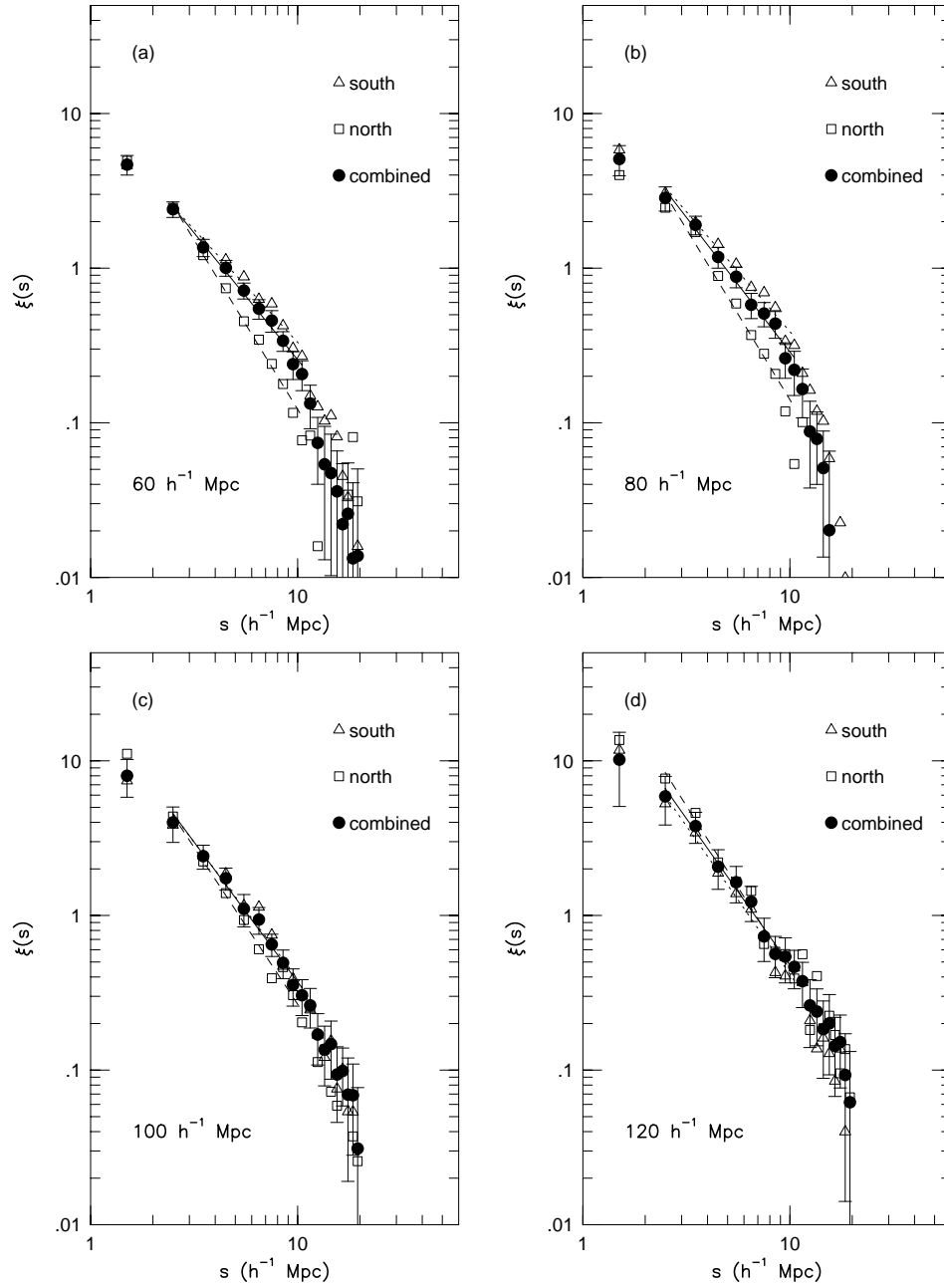


Fig. 6.— Comparison between the redshift correlation for the individual and combined samples for each volume limit. The solid line represents the power-law fit for the combined sample, the dotted line the fit for the south and the dashed line the fit for the north. Bootstrap error estimates are shown only for the combined sample.

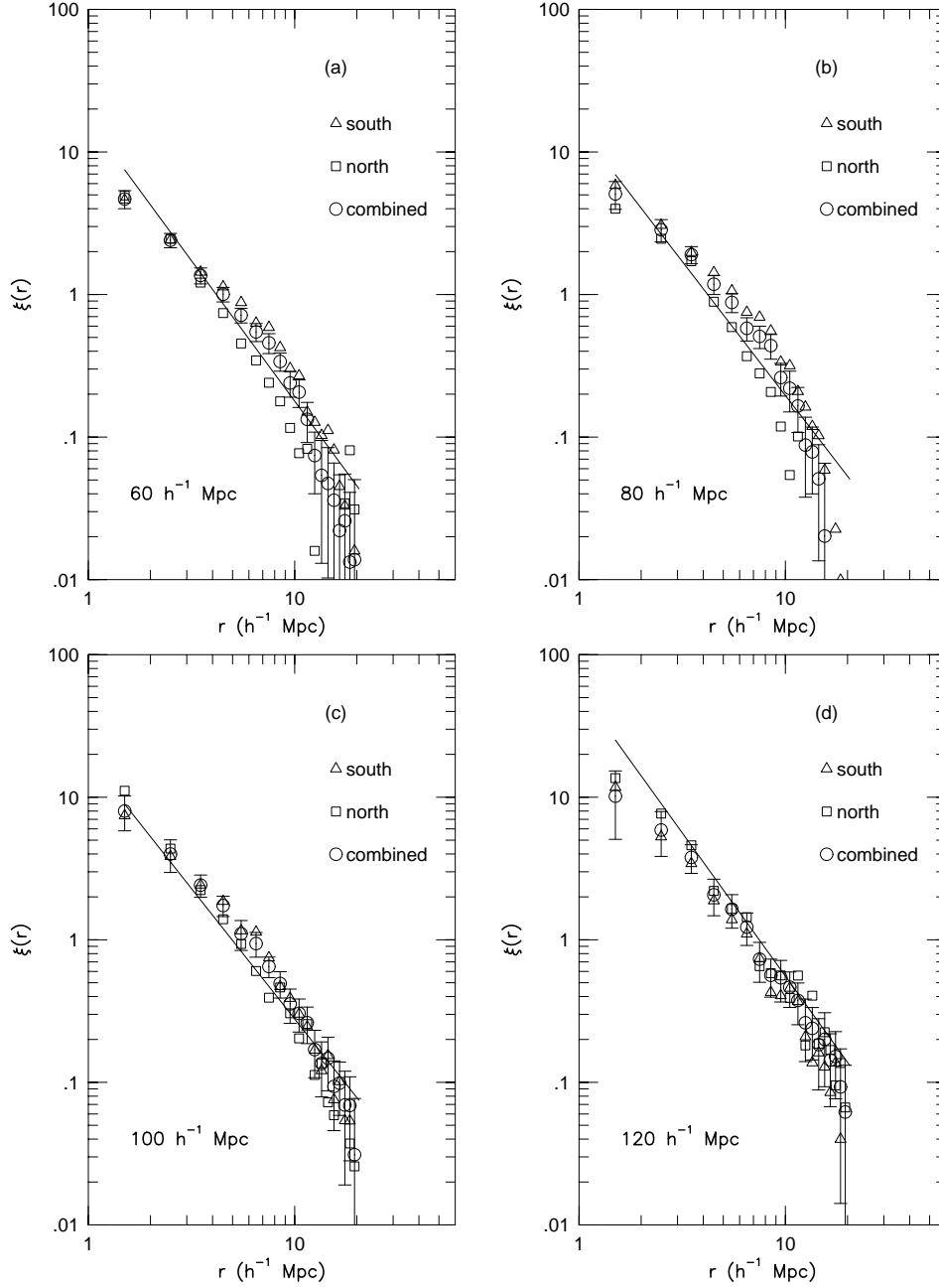


Fig. 7.— Comparison between the redshift space and real space correlation function, calculated for volume-limited samples. Open symbols represent the redshift space correlations, while solid lines represent the fits to the observed $\omega_p(r_p)$ using the power-law approximation of equation (11) for the combined sample. Error bars are shown only for the combined sample.

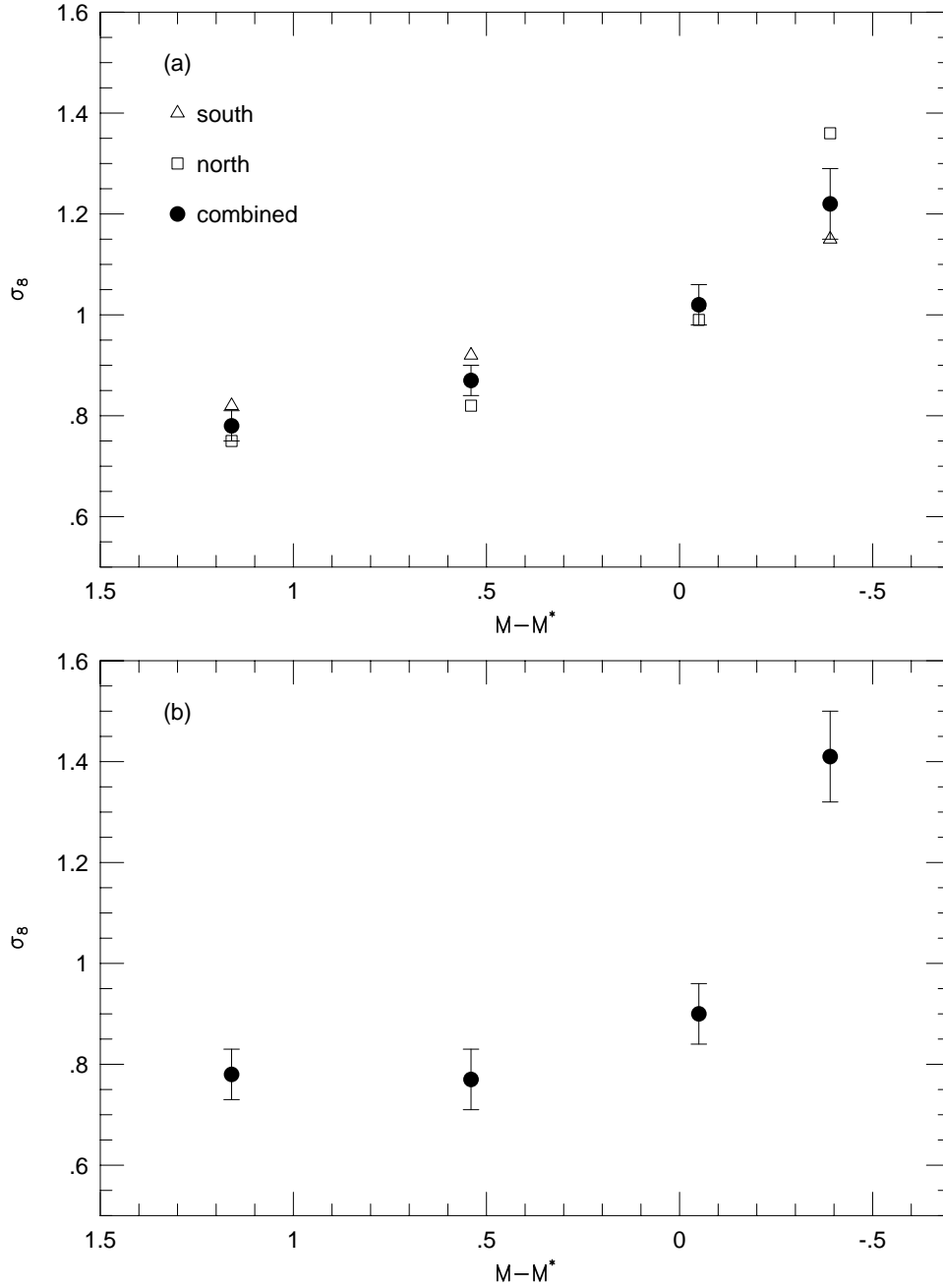


Fig. 8.— Dependence of the variance as measured through σ_8 on the galaxy luminosity using the correlation function measured in redshift space (panel a) and real space (panel b). In both panels the reference luminosity corresponds to the sample with $L \sim L^*$. The symbols in panel (a) represent galaxies of the SSRS2 south subsample (open triangles); SSRS2 north (open squares) and the combined sample (solid circle). The error bars were obtained by standard error propagation combining the bootstrap error estimates of the different samples, calculated at each of the separations shown in the plot. In panel (b) we only show the results obtained for the combined sample.

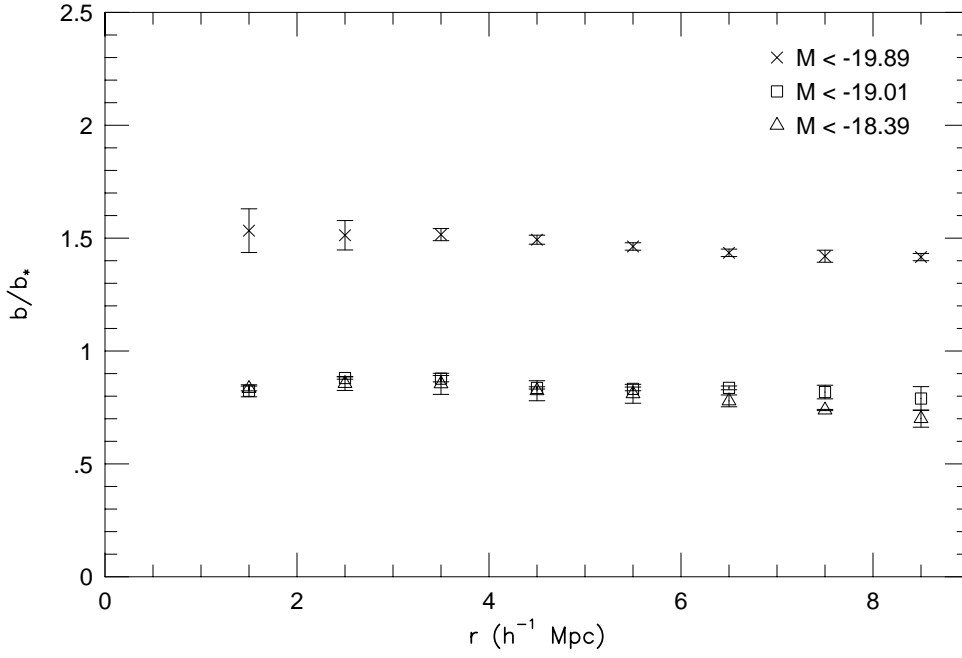


Fig. 9.— Variation of the relative bias between galaxies of different luminosities with scale, using the real space correlation function and equation (15). In this plot the reference luminosity corresponds to the sample with $L \sim L^*$. The symbols represent galaxies with $M \leq -19.89$ (crosses); $M \leq -19.01$ (squares) and $M \leq -18.39$ (triangles). The error bars were obtained by standard error propagation combining the bootstrap error estimates of the different samples, calculated at each of the separations shown in the plot.

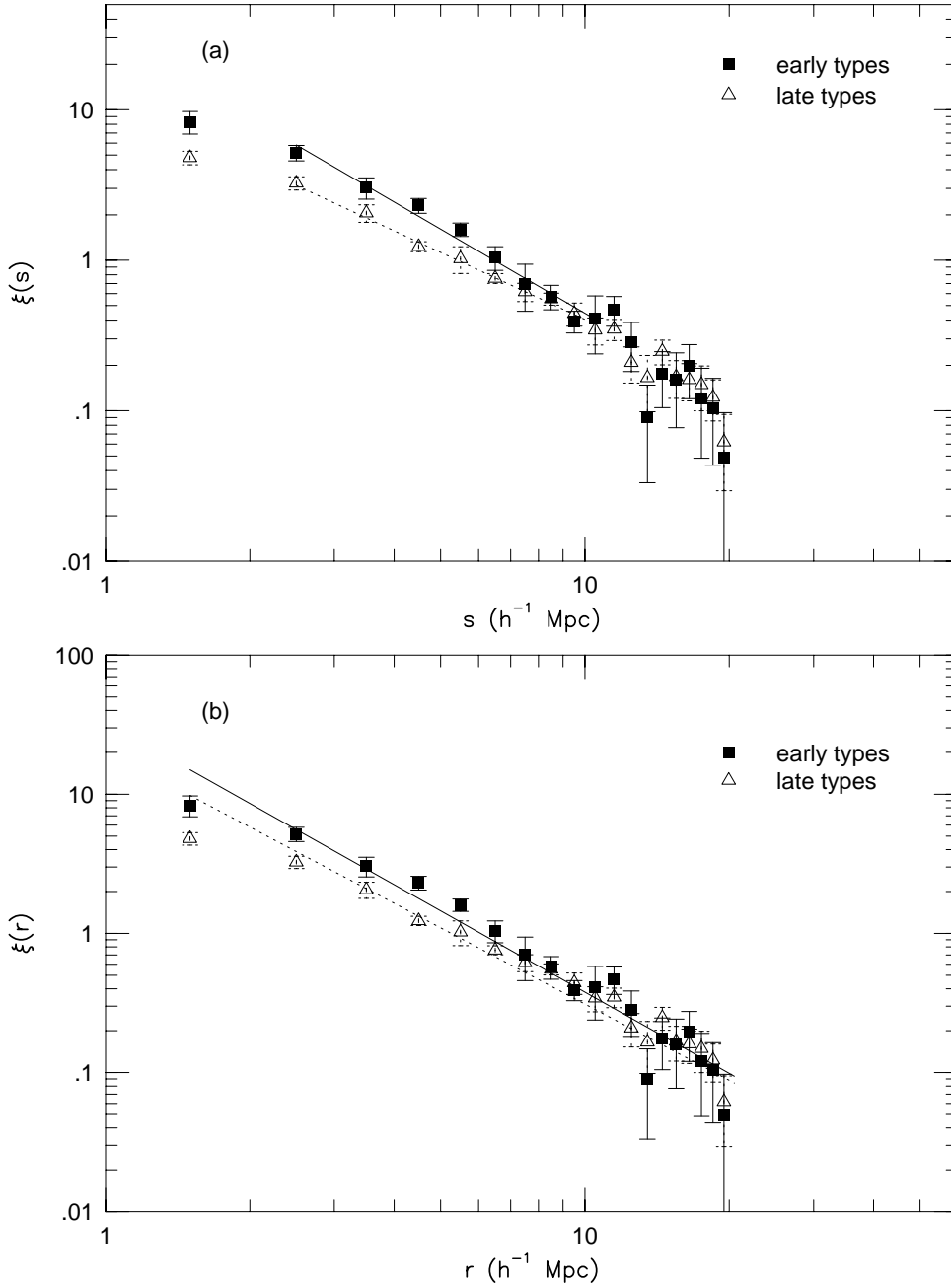


Fig. 10.— The two-point correlation for the SSRS2 discriminating morphological types calculated in redshift space (panel a). Solid squares represent early type galaxies and open triangles late types. The power-law fits are shown as solid and dotted lines respectively for early and late types. In panel (b) we show the points measured in redshift space together with the power-law fits measured in real space. The errors were estimated from the bootstrap resampling.

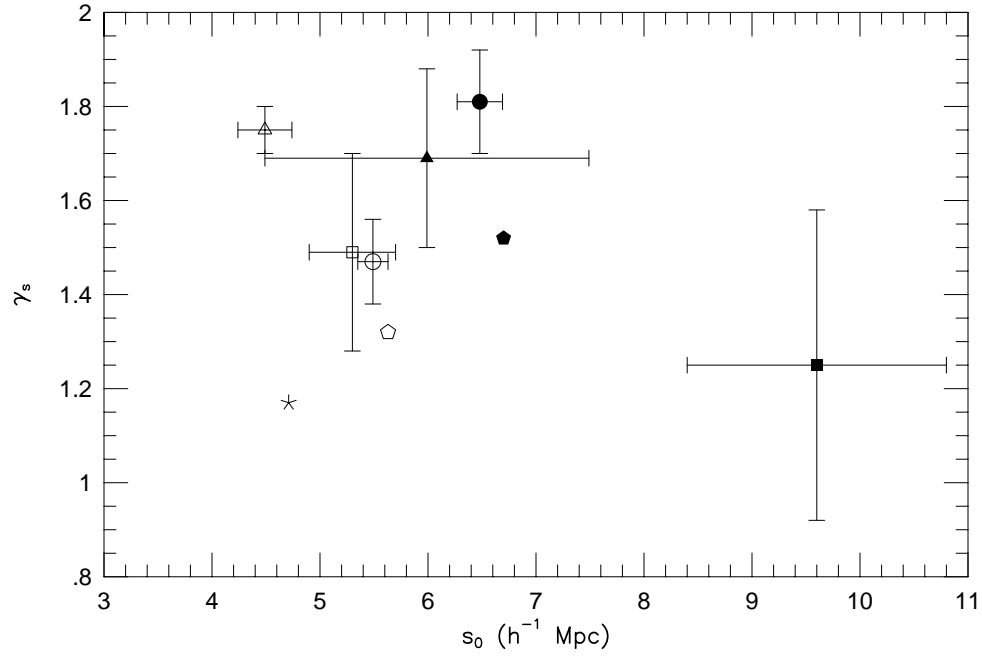


Fig. 11.— Comparison between values of s_0 measured in this paper for early types (solid circle) and late types (open circle), with measures of other works, presented in Table 5. These are the Stromlo-APM, represented as squares (solid for early types, open for late types), SSRS1 (solid and open triangles for early and late types respectively) and the ORS (early types as solid pentagon, Sa/Sb as open pentagon and Sc/Sd as a star). The error bars for the SSRS2 sample represent the statistical uncertainty obtained from the power-law fits.

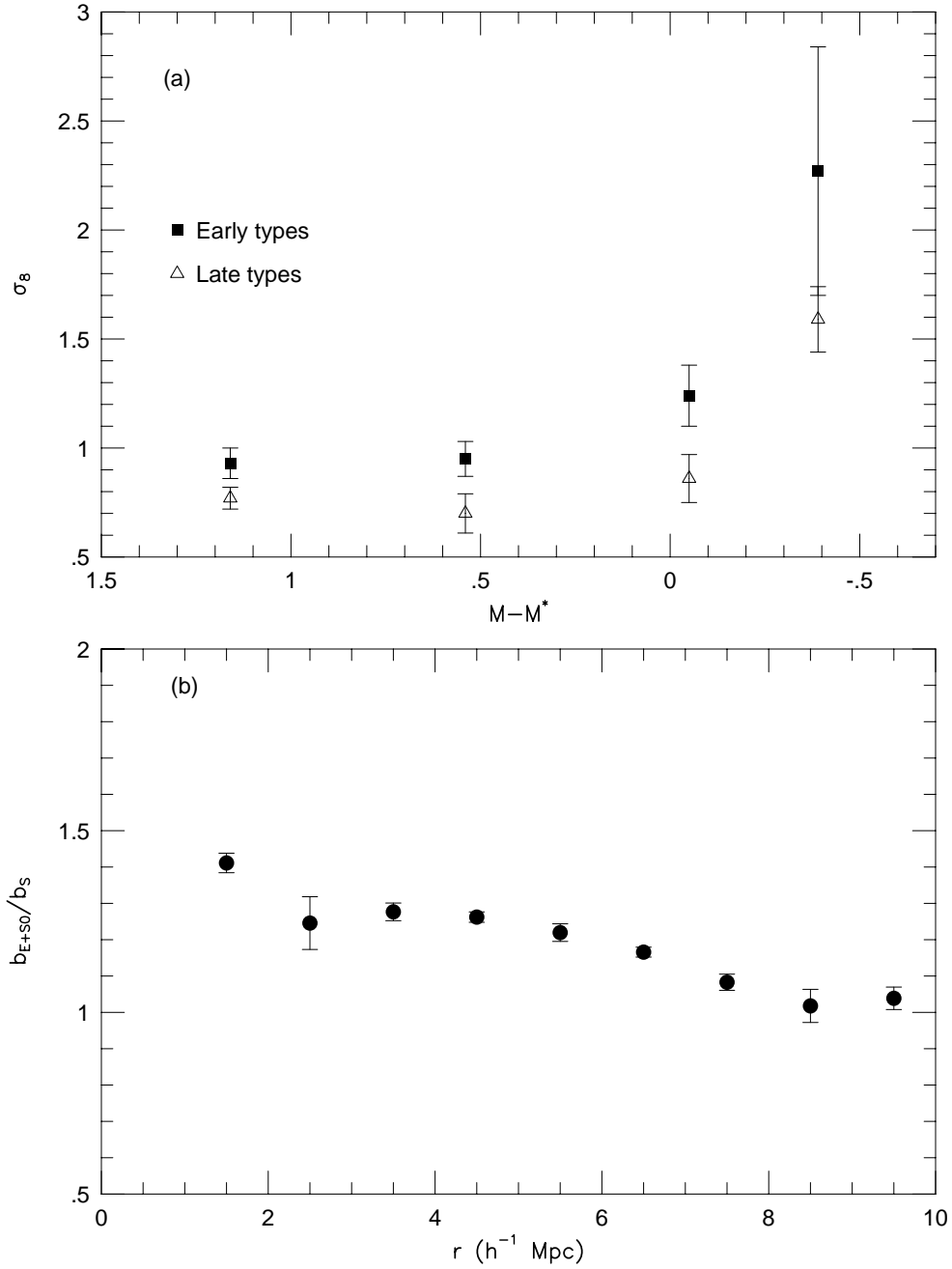


Fig. 12.— Biasing measures for galaxies discriminated by morphologies. Panel (a) shows the variance for different luminosity thresholds while panel (b) shows the relative bias between early and late types as a function of scale, using equation (16). In both panels these measures are derived from the real space correlation function. The error bars were derived through standard error propagation, using in panel (a) the estimated errors of the parameters obtained calculating the power-law fits, while in panel (b) they were obtained combining the bootstrap error estimates of both samples, calculated at each of the separations shown in the plot.

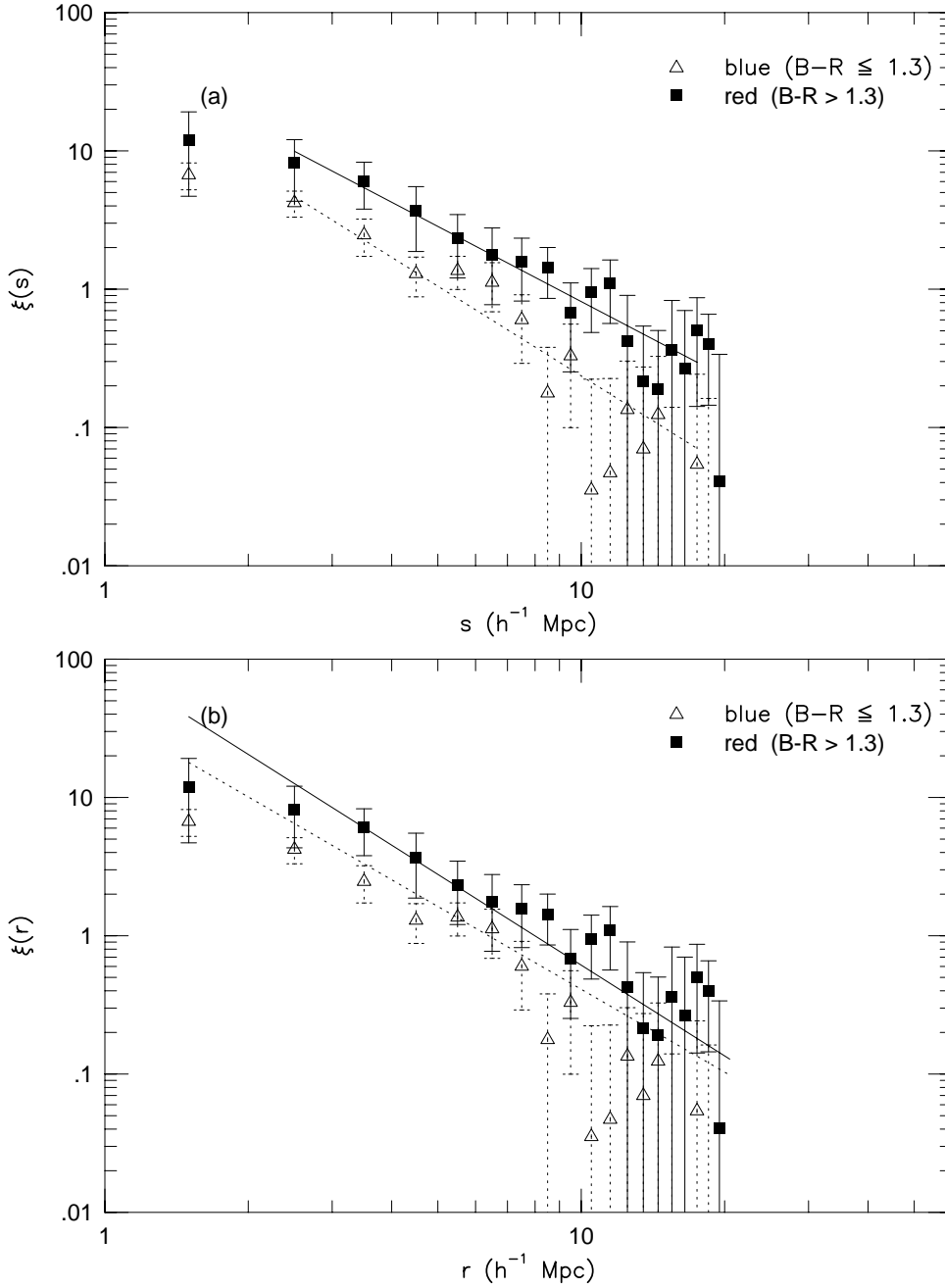


Fig. 13.— Panel (a) shows the redshift space correlation for galaxies discriminated now by colors. Table 8 shows the correlation parameters for these fits. Panel (b) shows the real space correlation for galaxies discriminated by colors. The points show the redshift-space correlation. Table 8 also shows the correlation parameters for these fits. The error bars were obtained by bootstrap resampling.

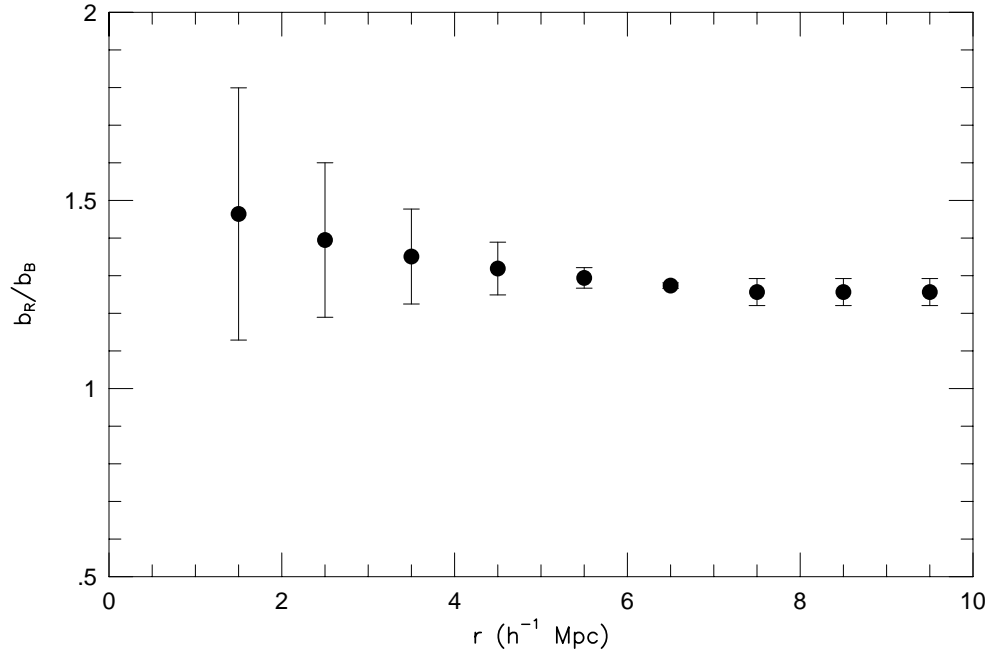


Fig. 14.— Relative bias between galaxies with red and blue colors as a function of scale, using the fits to $\xi(r)$. The error bars were obtained combining the statistical errors obtained in the power-law fits using standard error propagation.

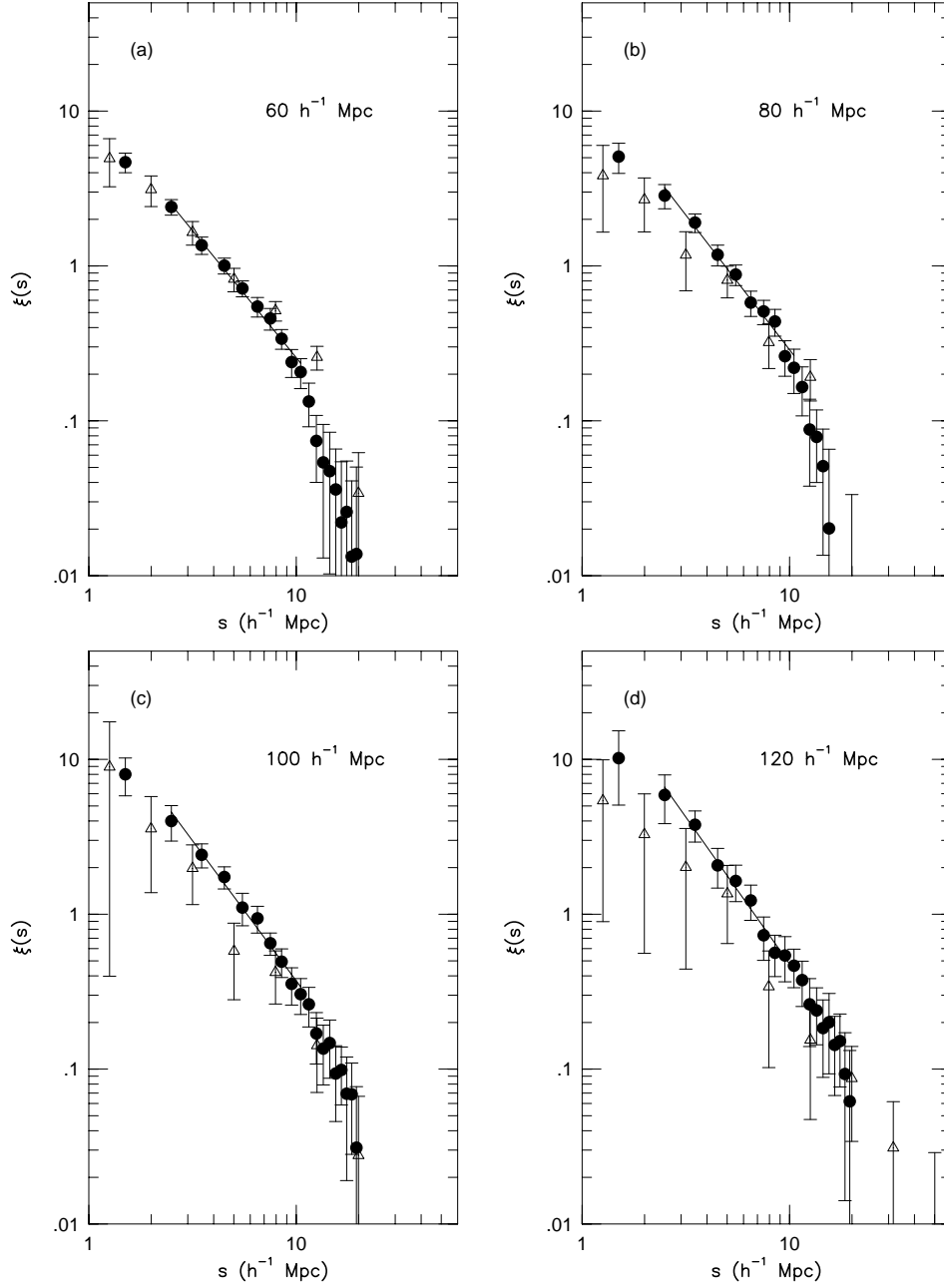


Fig. 15.— Comparison between the redshift correlation of the combined SSRS2 sample (solid circles) with that measured for *IRAS* galaxies (open triangles), for the different volume limits indicated in the panels. We also show the fits calculated for the SSRS2 sample. The error bars for both SSRS2 and *IRAS* subsamples were estimated using bootstrap resampling.

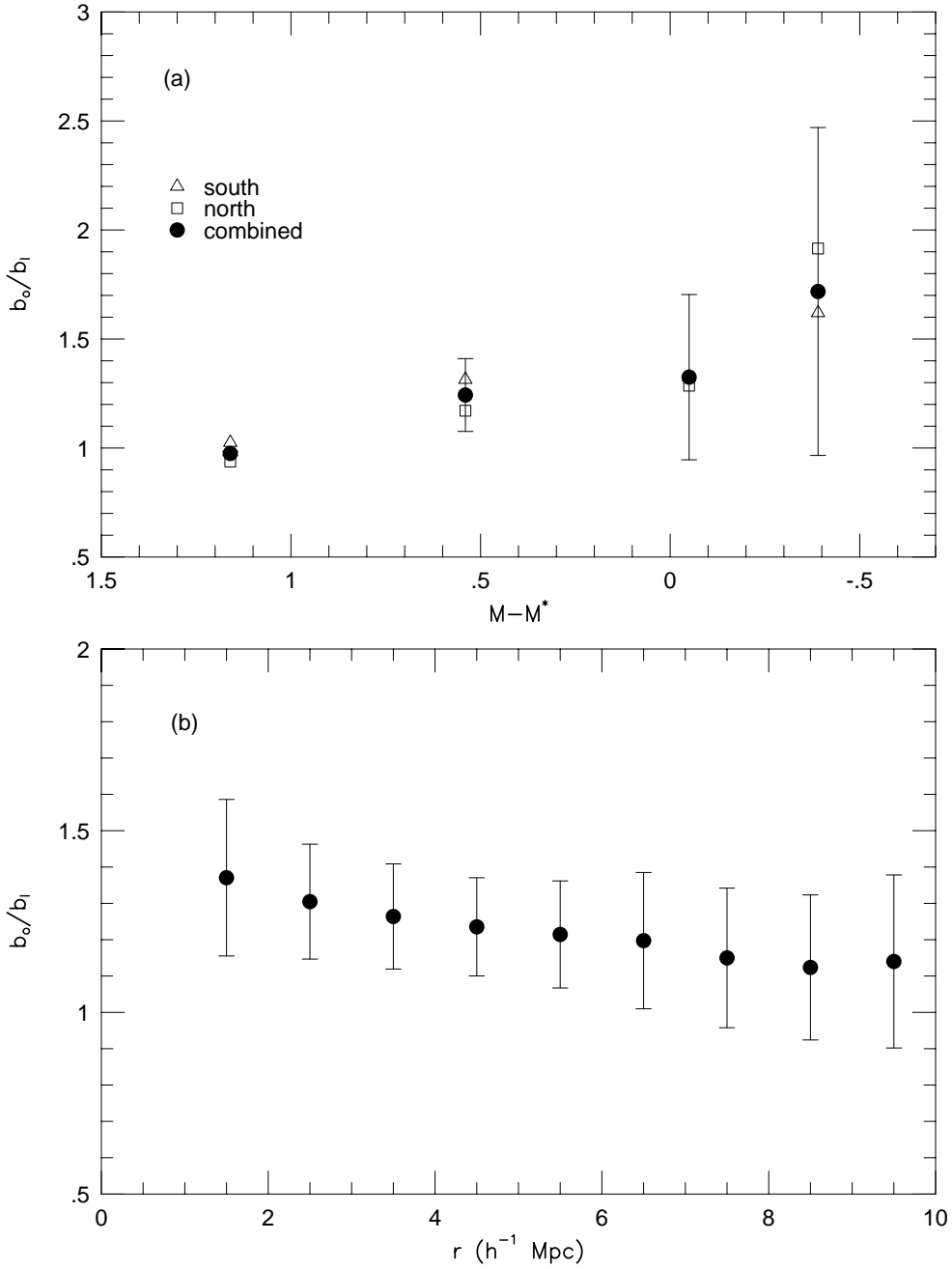


Fig. 16.— Panel (a) shows the relative bias between optical and *IRAS* galaxies as a function of luminosity, derived from the redshift space correlation function. The symbols represent the relative bias obtained considering the SSRS2 south (open triangles), SSRS2 north (open squares) and the combined sample (solid circle). Panel (b) presents the relative bias as a function of scale, but now using the real space correlation function. The error bars were obtained combining the σ_8 uncertainties for both samples (panel a), or by combining the correlation function bootstrap error at each separation in the case of panel (b). The large errors seen in panel (b) reflect the larger uncertainty that is obtained when calculating the correlation function in real space.

TABLE 2. Correlation function parameters measured by other authors

Survey	s_0 (h^{-1} Mpc)	γ_s	r_0 (h^{-1} Mpc)	γ_r	sample	ref.
(1)	(2)	(3)	(4)	(5)	(6)	(7)
<i>IRAS</i> 1.2 Jy	4.53±0.22	1.28±0.04	3.76±0.22	1.66±0.11	all	Fisher et al. 1994
LCRS	6.28±0.27	1.52±0.03		Tucker et al. 1996
Stromlo-APM	5.9± 0.3	1.47±0.12	5.1±0.2	1.71±0.05	all	Loveday et al. 1995
SSRS2	5.08±0.23	1.85±0.06	south	Marzke et al. 1995
CfA1	5.4±0.3	1.77±0.04	all	Davis & Peebles 1983
CfA2	7.5±1.7	1.6±0.1	all	de Lapparent et al.1988
Perseus-Pisces			8.4±0.8	2.05±0.09	early types	Guzzo et al. 1997
Perseus-Pisces			5.6±0.4	1.73±0.08	late types	Guzzo et al. 1997
Stromlo-APM	9.6±1.2	1.25±0.33	5.9±0.7	1.85±0.13	early types	Loveday et al. 1995
Stromlo-APM	5.3±0.4	1.49±0.21	4.4±0.1	1.64±0.05	late types	Loveday et al. 1995
SSRS1	5.99±1.50	1.69±0.19	early types	Santiago & da Costa 1990
SSRS1	4.49±0.25	1.75±0.05	late types	Santiago & da Costa 1990
ORS	6.70	1.52	early types	Hermit et al.1996
ORS	5.63	1.32	Sa/Sb types	Hermit et al.1996
ORS	4.71	1.17	Sc/Sd types	Hermit et al.1996
<i>IRAS</i> 1.2 Jy	4.54±0.35	1.31±0.10	60 h^{-1} Mpc	Fisher et al. 1994
<i>IRAS</i> 1.2 Jy	3.73±0.40	1.38±0.14	80 h^{-1} Mpc	Fisher et al. 1994
<i>IRAS</i> 1.2 Jy	4.27±0.51	1.68±0.33	100 h^{-1} Mpc	Fisher et al. 1994
<i>IRAS</i> 1.2 Jy	3.91±0.86	1.69±0.49	120 h^{-1} Mpc	Fisher et al. 1994

TABLE 3. Redshift space correlation parameters for volume-limited samples.

Sample	R (h^{-1} Mpc)	N_g	n ($\times 10^{-3} h^{-3}$ Mpc 3)	s_0 (h^{-1} Mpc)	γ_s	σ_8
(1)	(2)	(3)	(4)	(5)	(6)	(7)
South	60	780	9.59	4.69 ± 0.19	1.46 ± 0.13	0.82 ± 0.03
	80	762	3.95	5.44 ± 0.22	1.55 ± 0.14	0.92 ± 0.03
	100	821	2.18	5.86 ± 0.27	1.77 ± 0.17	1.02 ± 0.05
	120	619	0.95	6.33 ± 0.41	1.92 ± 0.27	1.15 ± 0.08
North	60	411	9.97	3.83 ± 0.17	2.19 ± 0.20	0.75 ± 0.04
	80	495	5.07	4.12 ± 0.19	2.21 ± 0.24	0.82 ± 0.04
	100	359	1.88	5.21 ± 0.37	2.03 ± 0.33	0.99 ± 0.07
	120	238	0.72	6.84 ± 0.65	2.12 ± 0.42	1.36 ± 0.15
Combined	60	1191	9.72	4.36 ± 0.13	1.64 ± 0.10	0.78 ± 0.03
	80	1257	4.33	4.88 ± 0.17	1.74 ± 0.14	0.87 ± 0.03
	100	1180	2.08	5.79 ± 0.22	1.81 ± 0.16	1.02 ± 0.04
	120	857	0.87	6.77 ± 0.36	1.90 ± 0.21	1.22 ± 0.07

TABLE 4. Real space correlation parameters, volume-limited samples.

Sample	R_{max} (h^{-1} Mpc)	r_0 (h^{-1} Mpc)	γ_r	σ_8
(1)	(2)	(3)	(4)	(5)
South	60	4.06 ± 0.28	1.82 ± 0.21	0.74 ± 0.06
	80	4.48 ± 0.32	1.92 ± 0.23	0.82 ± 0.06
	100	4.93 ± 0.47	1.89 ± 0.31	0.90 ± 0.09
	120	6.83 ± 0.46	2.04 ± 0.28	1.31 ± 0.10
North	60	4.04 ± 0.30	2.18 ± 0.34	0.79 ± 0.06
	80	3.96 ± 0.48	1.88 ± 0.33	0.73 ± 0.10
	100	5.89 ± 0.54	1.86 ± 0.31	1.05 ± 0.10
	120	10.10 ± 1.11	2.29 ± 0.36	2.37 ± 0.35
Combined	60	4.17 ± 0.24	1.97 ± 0.20	0.78 ± 0.05
	80	4.20 ± 0.33	1.88 ± 0.22	0.77 ± 0.06
	100	4.97 ± 0.34	1.83 ± 0.20	0.90 ± 0.06
	120	7.47 ± 0.42	2.01 ± 0.21	1.41 ± 0.09

TABLE 5. Correlation function parameters for different morphologies.

Sample	s_0 (h^{-1} Mpc)	γ_s	σ_8	r_0 (h^{-1} Mpc)	γ_r	σ_8
(1)	(2)	(3)	(4)	(5)	(6)	(7)
Combined early types	6.46 ± 0.20	1.86 ± 0.11	1.15 ± 0.04	6.06 ± 0.39	1.94 ± 0.21	1.11 ± 0.07
Combined late types	5.42 ± 0.13	1.48 ± 0.09	0.92 ± 0.02	5.26 ± 0.37	1.82 ± 0.17	0.94 ± 0.06

TABLE 6. Redshift space correlation parameters for volume-limited sub-samples divided in morphologies.

Sample	R (h^{-1} Mpc)	N_g	n ($\times 10^{-3} h^{-3}$ Mpc 3)	s_0 (h^{-1} Mpc)	γ_s	σ_s
(1)	(2)	(3)	(4)	(5)	(6)	(7)
Early	60	395	3.22	5.16 ± 0.27	1.68 ± 0.19	0.90 ± 0.05
Early	80	418	1.44	6.15 ± 0.34	1.82 ± 0.20	1.08 ± 0.06
Early	100	372	0.66	6.68 ± 0.47	2.11 ± 0.31	1.32 ± 0.11
Early	120	272	0.28	7.17 ± 0.79	2.24 ± 0.50	1.55 ± 0.22
Late	60	778	6.35	4.05 ± 0.18	1.62 ± 0.14	0.73 ± 0.04
Late	80	810	2.79	4.20 ± 0.22	1.71 ± 0.18	0.76 ± 0.04
Late	100	774	1.36	5.39 ± 0.31	1.72 ± 0.21	0.94 ± 0.05
Late	120	566	0.58	6.76 ± 0.55	1.60 ± 0.28	1.11 ± 0.09

TABLE 7. Real space correlation parameters, volume-limited samples.

Sample	R_{max} (h^{-1} Mpc)	r_0 (h^{-1} Mpc)	γ_r	σ_s
(1)	(2)	(3)	(4)	(5)
Early	60	5.10 ± 0.38	1.91 ± 0.26	0.93 ± 0.07
Early	80	5.27 ± 0.46	1.86 ± 0.29	0.95 ± 0.08
Early	100	5.73 ± 0.56	2.30 ± 0.46	1.24 ± 0.14
Early	120	8.60 ± 1.44	2.45 ± 0.71	2.27 ± 0.57
Late	60	3.89 ± 0.24	2.21 ± 0.28	0.77 ± 0.05
Late	80	3.81 ± 0.45	1.85 ± 0.28	0.70 ± 0.09
Late	100	4.83 ± 0.61	1.72 ± 0.29	0.86 ± 0.11
Late	120	8.12 ± 0.59	2.08 ± 0.30	1.59 ± 0.15

TABLE 8. Correlation function parameters, for different colors.

Sample	s_0 (h^{-1} Mpc)	γ_s	σ_s	r_0 (h^{-1} Mpc)	γ_r	σ_r
(1)	(2)	(3)	(4)	(5)	(6)	(7)
Red galaxies 14.5	8.92 ± 0.85	1.81 ± 0.26	1.51 ± 0.16	7.99 ± 0.95	2.18 ± 0.45	1.67 ± 0.25
Red galaxies 14.2	10.75 ± 1.57	1.62 ± 0.28	1.62 ± 0.25
Blue galaxies 14.5	5.12 ± 0.33	2.16 ± 0.25	1.01 ± 0.07	6.39 ± 0.50	1.99 ± 0.29	1.19 ± 0.10
Blue galaxies 14.2	5.20 ± 0.41	1.79 ± 0.26	0.92 ± 0.07